university of groningen / faculty of science and engineering

Novel polymerized ionic liquid for solid polymer electrolyte application

2-Acrylamido-2-methylpropane sulfonic acid tested as polymerized ionic liquid in a grafted triblock-copolymer for solid polymer electrolyte application

Supervisor:
dr. P. Raffa

Second assessor:
dr. V. Kyriakou

Daily supervisor:
A. Guzik

Author:
Reinier B. Goldhoorn

June 23, 2023

Abstract

Block co-polymers have recently drawn more attention for potential application as solid polymer electrolytes (SPE) in metal anode lithium-ion batteries. Their nature to self-assemble into a supra-molecular structure could mean that the soft conductive and hard structural parts could be a best of both worlds for conductivity of ions and the structural strength to prevent dendrite formation. In this research PSt-*b*-PEGMA-*r*-AMPS-*b*-PSt, polymerized with protonated Et_3N and neutralized with LiOH, has been synthesized using RAFT-polymerization and tested for application on ionic conductivity for potential SPE application in lithium-ion batteries. Here, the influence of AMPS as an embedded anionic part within the polymer backbone is investigated based on the ratio of AMPS to PEGMA and also the possibility to neutralize the AMPS with LiOH in MQ-water. For all the produced polymers, the PSt parts have the same size due to the utilization of the DMAcTTC-RAFT-agent which made propagation from the middle possible. Due to the poor solubility of the chain extended polymers, it was impossible to find the molecular weight of the polymers by GPC, however, the GPC on the macroCTA was possible. The added amounts of monomer together with the conversion (obtained with ^{1}H-NMR) was used to determine the molecular weight. DOSY was used to investigate the dispersion and ICP-MS to confirm the neutralization of AMPS by LiOH. The decomposition temperature for all the polymers was found by using TGA, which was found to be around 150 °C. DSC was used to determine the T_g which was in accordance with literature around −60 °C. Electrochemical impedance spectroscopy (EIS) was then applied on two polymers to find the correlation of [EO]:[Li^+] and temperature to the ionic conductivity. PSt_{27}-*b*-$PEGMA_{156}$-*r*-$AMPS_{54}$-*b*-PSt_{27} was found to have the highest conductivity of 8.720×10^{-7} S cm^{-1} at 115 °C with a [EO]:[Li^+] of 30:1.

Contents

Acronyms

^{1}H-NMR Proton nuclear magnetic resonance. 1, 18–20, 23, 25–28, 32, 34, 40, 53, 62–64

^{13}C-NMR Carbon-13 NMR. 3, 23, 40

ACVA 4,4'-Azobis(4-cyanopentanoic acid). 18–20

AMPS 2-Acrylamido-2-methylpropane sulfonic acid. 1–3, 12–14, 18, 20, 22, 27–29, 32, 33, 37, 38, 42, 43, 45, 53, 62–66, 81

BEV battery-electric-vehicles. 7

$CDCl_3$ Deuterated Chloroform. 18–20, 23, 27, 28

CHNS-analysis CHNS elemental analysis. 4, 24, 32, 66

CTA chain-transfer-agent. 1–3, 11, 18–20, 23, 25–29, 39, 53

DLC diffusion-limited C-rate. 8

DMAcTTC S,S'-Bis(a,a'-dimethyl-a"-acetic acid)trithiocarbonate. 1, 18, 25, 53

DMSO-d_6 Deuterated Dimethylsulfoxide. 18

DOSY Diffusion ordered spectroscopy. 1, 3, 4, 23, 39, 53, 72–74

DP degree of polymerization. 13, 14, 19, 20, 26–29, 51

DSC Differential scanning calorimetry. 1, 3, 23, 41–43, 53

EIS Electrochemical impedance spectroscopy. 1–4, 14–17, 24, 47–50, 53, 82, 83

Et_3N Triethylamine. 1, 18, 20, 22, 28, 33–35, 39, 53, 79

GPC Gel Permeation Chromatography. 1, 4, 19, 23, 26, 27, 29, 39, 53, 60

GPE gel polymer electrolyte. 9, 10

ICP-MS Inductively coupled plasma mass spectrometry. 1, 3, 24, 34, 37, 38, 53

LiOH lithium-hydroxide. 1, 22, 33, 37, 38

MWCO molecular weight cut-off. 19

PDI Polymer Dispersity Index. 11, 14, 39, 53

PEG polyethylene glycol. 9, 10

PEGMA polyethylene glycol methyl acrylate. 1–3, 12, 13, 18–20, 27–29, 32, 37–39, 45, 53, 62–64, 66, 81

PEO Polyethylene oxide. 9, 13, 14, 43–45

PSt Polystyrene. 1, 19, 20, 23, 26, 27, 45, 53

QQ-HSQC Quick, quantitative hetero-nuclear correlation. 3, 4, 23, 40, 69–71

RAFT Reversible Addition Fragmentation chain-Transfer polymerization. 1, 11, 12, 14, 25, 27, 28, 53, 67, 68

RDRP Reversible Deactivation Radical Polymerization. 11

SEC Size-exclusion chromatography. 19

SEM Scanning Electron Microscopy. 3, 11, 24, 41, 44–46, 51, 52

SPE solid polymer electrolyte. 1, 2, 9, 13, 14, 16, 17, 41, 45, 53

T_g Glass transition temperature. 1, 16, 23, 41–43, 47, 51, 53

TEM Transmission electron microscopy. 41, 44, 45

$TFSI^-$ Bistriflimide. 13

TGA Thermogravimetric analysis. 1, 3, 4, 23, 24, 41–43, 53, 76

THF Tetrahydrofuran. 18, 19, 26

Glossary

dendrite deposition of solid lithium between the cathode and the anode causing a detrimental short-circuit. 1, 8

1 Introduction

From its inception, the lithium-ion battery became ubiquitous with virtually every mobile electronic device currently on the market. In 2019, the Royal Swedish Academy of Science rewarded three scientists the Nobel price in chemistry for their fundamental contributions to the development in the lithium-ion battery technology and with that the foundations to a fossil free society. [1] In 2021, the UN called the lithium-ion battery technology a "*critical pillar in a fossil fuel-free economy*". [2] The demand for this technology has exploded, with a demand increasing by 30% per annum to reach 4700 GWh by 2030.[3] The ever-increasing demand for energy storage capacity has made the scientific interest in new methods for storage increase likewise. [4] The main source for this surge in interest has been driven by the carbon-emission-neutral developments for battery-electric-vehicles (BEV) and grid energy storage solution.

1.1 Working principle of a battery

Lithium is the third element on the periodic table and is the lightest metal in the universe. It is an alkali-metal, meaning it has one electron in its outermost s-orbital and with that, possesses a low ionization energy. This means that lithium on itself easily oxidizes and is therefore not stable in a metallic form. At a discharged state, the lithium ions are trapped within a transition metal oxide ($LiMO_2$) with notable cathode material to be $LiCoO_2$, $LiMn_2O_4$, $LiFePO_4$, etc. The trapping of lithium ions is called lithium intercalation. [5] The cathode is the positive site of a battery, which is separated from the negative site of a battery by an electrolyte. An electrolyte only let through positively charged ions, which is relevant for the working principle. The electrolyte is filled with organic lithium salt which has a low dissociation energy, meaning lithium is able to attach and dettach easily. The anode (negative side of a battery) is mainly made up of graphite. When a (conventional) current is attached in the direction of the cathode, electrons are forced to move in the opposite direction (electron current). At the anode a reaction takes place where the graphite is lithiated. The net formula of a charge cycle is as follow:

During charge	**During discharge**
At the cathode:	At the anode:
$LiMO_2 \rightarrow Li^+ + e^- + MO_2$	$C_6Li \rightarrow Li^+ + e^- + C_6$
At the anode:	At the anode:
$Li^+ + e^- + C_6 \rightarrow C_6Li$	$Li^+ + e^- + MO_2 \rightarrow LiMO_2$
Overall formula:	Overall equation:
$LiMO_2 + C_6 \rightarrow MO_2 + C_6Li$	$MO_2 + C_6Li \rightarrow LiMO_2 + C_6$

The lithium is in an unstable state intercalated in the graphite. When a load is connected to the battery, the ions will move to the stabler cathode side in the metal oxide. Only the ions are able to move through the electrolyte, meaning the electrons have to bypass it causing a (conventional) current in the opposite direction where lithium is intercalated into the metal oxide again according to the following formula

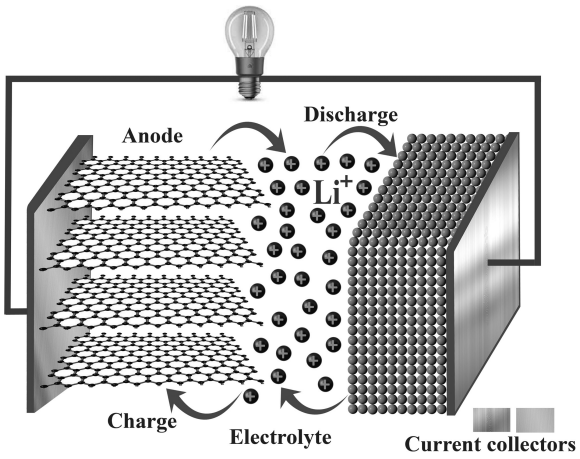

Figure 1: A schematic illustration on the working principle of a lithium ion battery. The charge and discharge cycles are depicted by arrows with the movement of the ions and electrons. Figure obtained from [6]

Spontaneous ignition of lithium-ion batteries is one of the many issues that have to be tackled in the near future for full electrification of society. The occurrence is low; however, the impact of these spontaneous fires is enormous. In the US alone, 19 people have died because of battery related fires in 2022. [7] The cause of fires is mainly short circuiting of the electrodes.

The inherent problem of a lithium-ion battery nowadays is that there is a tradeoff between safety and endurance against capacity and charge rate. Furthermore, there is a tradeoff between the powerdensity and energy density, which is called the diffusion-limited C-rate (DLC). [8] For instance, ideal anode material would be lithium metal which can bring a higher capacity to the battery. However, with increasing the density of charge, dendrite formation can occur. The exact kinetics of this formation is yet unknown, but the general consensus is that dendrite formation happens through the part of the electrolyte membrane where there is the least amount of mechanical strength. [9] Several methods to overcome this issue have been brought up, like solid electrolytes forming the now much pursued all solid state batteries. As mentioned, lack of mechanical strength is the main issue in the reason why dendrite formation is able to occur. An all solid system would be able to prevent deposition in the first place. Next, the mechanical strength will also increase one of the main safety concerns, namely short-circuit due to external influence. [10]

The solid state battery technology can be divided up into 3 categories, listed in figure 2, with the 1st category being the liquid electrolyte. In this report, an organic polymer-based compound will be treated and compared to the current liquid electrolyte technology.

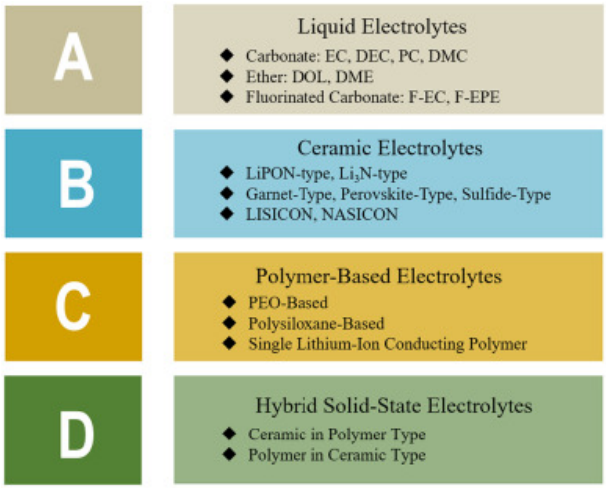

Figure 2: The 4 categories of electrolytes in lithium-ion technology. Figure obtained from [11]

1.2 Solid polymer-based electrolytes

Polyethylene oxide (PEO) (in most literature referred to as polyethylene glycol (PEG)) is intensively investigated over the past 5 decades as a useful candidate for high capacity ion-battery application. [12, 6] It is able to dissolve a wide variety of lithium salts and also to transport lithium-ions through its membrane via the segmental motion mechanism explained in figure 4. The reason why PEO did not catch on as a solid polymer electrolyte (SPE) is because it is inherent to crystallize at room temperature which inhibits the segmental motion. A method to overcome this is to add a plasticizer so that the substance would become more amorphous, or even gel-like (gel polymer electrolyte (GPE)). [13] The downside of adding such plasticizer is reduction of mechanical strength and with that loss in benefits compared to simpler conventional liquid electrolytes. In order to keep the high lithium ion conductivity through the membrane on one hand and improve mechanical strength on the other hand remains a challenge, because until now this remains a trade-off between the two. [14] This is illustrated in figure 3. The goal is to find a way to support the amorphous part of the membrane through structural rigidity of either a filler, another polymer or designing a polymer that inherently possesses this capability.

1.2.1 Blend polymer electrolyte

Blending PEO with either a polymeric plasticizer or polymer matrix for enhancing mechanical strength is a pursued over the years for it theoretically being the easiest method for manipulating the strength and conductivity. The theory is that crystallization of PEO is hindered, but retain the modulus of non-influenced PEO. [6, 13] Experimental studies have shown that the crystallization of the PEO is hindered to a certain degree, however processability is limited as well.

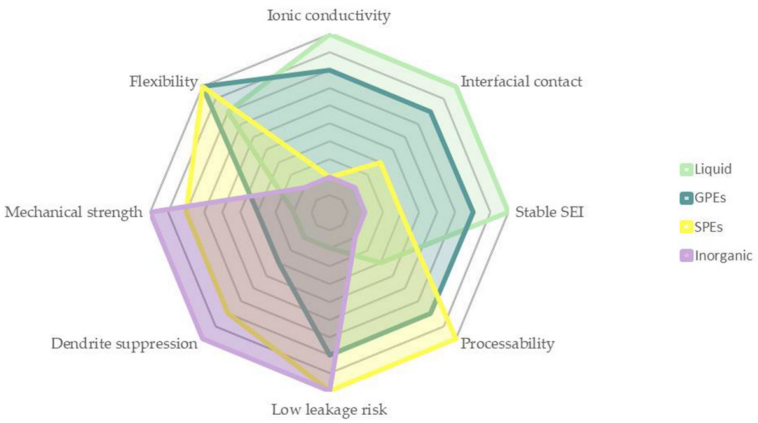

Figure 3: The trade-of between the different electrolyte technologies. The hybrid variant is not depicted and the GPE variant is shown here, clearly pointing out the mechanical strength issue. Figure obtained from [14]

1.2.2 Block co-polymer

Block co-polymers are becoming more interesting based on the ability of these polymers to self assemble into supra-molecular structure based on for instance hydrophilicity. Co-polymers have a lower tendency to crystallize compared to their homo-polymer counterparts, experiments have shown. Numerous examples have been tested for di-block polymers [6, 13] This is phenomena is enhanced by the segregation strength of the incorporated blocks. [15]

1.2.3 Grafted co-polymer

Interference of the crystallization can also occur via another method, namely grafted polymer chains which will create a brush like structure preventing the polymeric backbones to align. Chain end-groups of the grafted ethylene oxide are in theory more mobile than linear polyethylene.

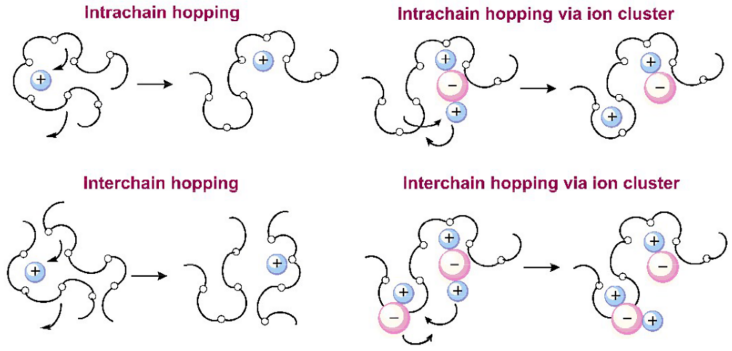

Figure 4: Segmental motion of lithium-ions through the PEG-membrane. Figure obtained from [13]

1.3 Supramolecular structures

A polymer that has both hydrophilic and hydrophobic domains will selfassemble by alignment of these phases. A certain ratio of polystyrene together with polyethylene oxide within the same polymer chain is proven to cause the phases to be separated in solid form. [16] As is seen in figure 5a, the hydrophobic phase will form a backbone structure that will give mechanical strength to the membrane. The hydrophilic part is in the middle and will be the conductive part of the ions. First research into these structures for battery electrolyte applications was done by Ruzette et al. [17] The ionic conductivity they observed was, in phase separated appearance, $5.6 \times 10^{-5}\,\mathrm{S\,cm^{-1}}$. Niitani et al. continued on this same principle, but produced a triblock-copolymer to prevent chain mobility of the hydrophilic part and introduce mechanical strength. They've found an ionic conductivity of $2 \times 10^{-4}\,\mathrm{S\,cm^{-1}}$ which is higher compared to the Ruzette et al. yet also possesses more mechanical strength.

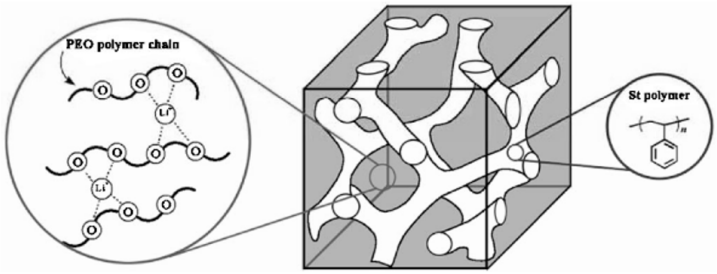

(a) Theoretical supramolecular structure.

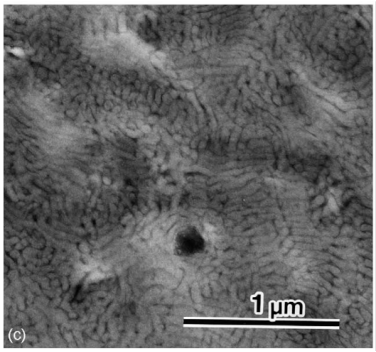

(b) Supramolecular structure as seen on SEM.

Figure 5: The supramolecular structure in theory and on SEM. Figures are obtained from [16]

1.4 RAFT-polymerization

Reversible Addition Fragmentation chain-Transfer polymerization (RAFT) is a form of Reversible Deactivation Radical Polymerization (RDRP) where through '*living chain*' mechanism the PDI, complex molecular architectures, capacity for continued chain growth and high-end fidelity can be steered and controlled. [18] This technique becomes interesting when one is interested in producing block-co-polymers with enhanced capabilities. Over the past 25 years this technique has been used to develop a variety of polymers with complex architecture finding its application in medicine[19], complex coacervates [20], surfactants and supramolecular assembled polymer membranes. [21, 22] RDRP is based on the principle of equilibrium between active and dormant chains which activates in the presence of a radical, in this case a radical initiator. Because of the need for a radical initiator for the polymerization to propagate, its also called degenerative transfer since the overall number of radicals is not changing due to the activation-deactivation process of the initiator on the living chain. The radical species will attach to the RAFT-agent, or the chain-transfer-agent (CTA). A schematic oversight for the mechanism can be found in figure 6. In step I the radical initiator will be

activated by its activation source, mostly heat (≥80 °C). In step II, the the initiator will radically initiate the dormant species (monomer) to react with the RAFT-agent forming an equilibrium reaction between the active species attached to the RAFT-agent and the chain end group attached to the RAFT-agent. In step IV the radical RAFT-end group will initiate another dormant species (monomer) which will then attach to the RAFT-end group (step V) similar to step III. This process continues until termination which occurs by disproportionation and decrease in temperature (<80 °C).

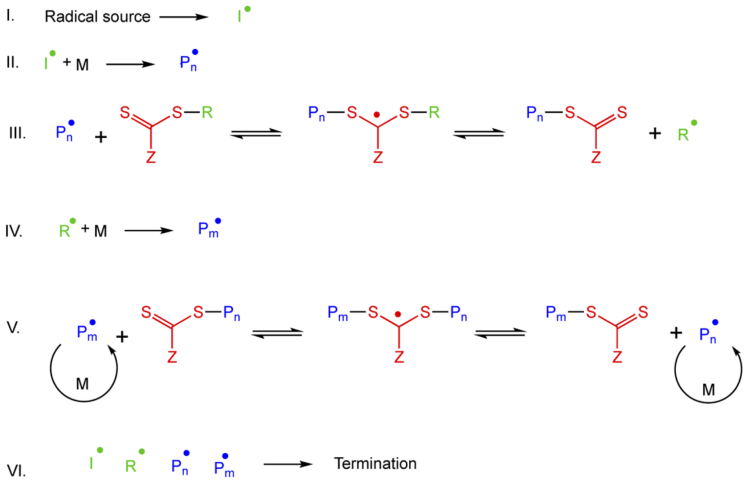

Figure 6: The proposed mechanism for Reversible Addition Fragmentation chain-Transfer polymerization (RAFT). Figure obtained from [18]. A more detailed outlook can be found in appendix A.6 (page 66).

1.5 Polymer design

Sadoway et al. investigated grafted block copolymers for battery application as one of the first. [23] They used POEM-b-PLMA as polymer chain with $LiCF_3SO_3$ as lithium salt. Their salt concentration depended on the amount of ethylene oxide that would be influencing the conductivity. Niitani et al. investigated triblock copolymers as a mean to increase the mechanical strength and saw that there is a relationship between the amount of styrene compared to the ethylene oxide for introducing phase separation. The hydrophilic monomer within their chain was PEGMA and the hydrophobic being styrene. [16] Their choice of salt was $LiClO_4$ which did not have any plasticizer effect, but they received a competitive ionic conductivity of $2\times10^{-5}\,\mathrm{S\,cm^{-1}}$ nevertheless. Beaudoin et al. investigated the molecular weight of the polymer on the melting temperature and ionic conductivity. [24] All the highlighted researches had a supramolecular structure and the design of the polymers that are to be tested in this report will consist of that same structure based on phase separation. These reports investigated with a blended lithium salt, meaning the salt is blended, or doped in, after polymerization. Bouchet et al. were on of the first to incorporated the LiTFSI salt within the polymer chain. [25] This is an anionic block that also adds a plasticizing effect to the structure making the hydrophilic part more mobile. Gunday et al. were, as far as we are aware of, the first to test AMPS as a lithium salt incorporated within the polymer chain. [26] They did not add any other lithium salt to the mix but were able to observe lithium conductivity nonetheless.

$TFSI^-$ is a widely investigated ionic liquid that can act as a lithium salt within a battery electrolyte, but also to act as a plasticizer. All the above-mentioned investigations into supramolecular structures that also contained the $TFSI^-$ anion, noticed an increase in ion conductivity. Investigating the addition of this salt into the tested triblock-copolymer could benefit the conductivity.

Size

The DP of the blocks is based on the research done by Beaudoin et al. [24] In this research it was found that the DP of styrene around 2×30 and PEO around 200 is the most ideal for ionic conductivity of lithium.

Composition

Multiple reports found that there is a relationship between the ratio of [EO]:[Li] and the ion conductivity which is at optimum between 10:1 and 20:1. This has to do with the vacant oxygen sites of the PEO chain, but also that lithium is needed to promote inter-chain hopping. [24, 27, 6, 28] The used PEGMA in this research has a molecular weight of $500\,\mathrm{g\,mol^{-1}}$, meaning the DP of EO within this monomer is 8-9. When a polymer containing 50:50 [AMPS]:[PEGMA] it has a [EO]:[Li] ratio of 8:1, for instance. In other words, this [AMPS]:[PEGMA] ratio should be in theory the best according to the aforementioned reports. The ratio between AMPS and PEGMA is an important part of this research.

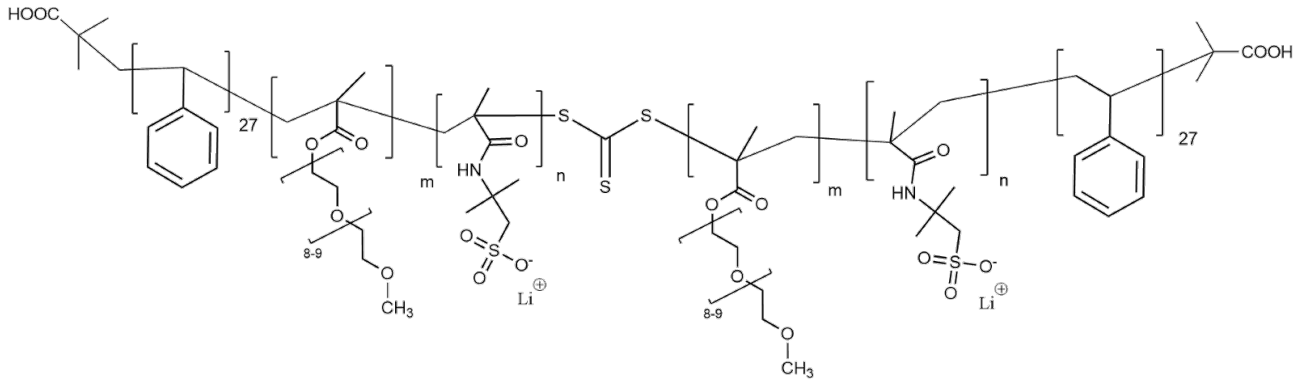

Figure 7: The desired polymer structure

1.6 Research question

AMPS could be an interesting candidate to investigate as embedded anion in the polymer backbone of a solid polymer electrolyte (SPE). Next, mechanical strength and hindering of the crystal phase at the same time can be achieved by producing triblock copolymers with a hard-soft-hard formation which is

already investigated. [23, 27, 29] Furthermore, grafted monomers are also investigated and benefits the ionic conductivity as well. [27] Reversible Addition Fragmentation chain-Transfer polymerization (RAFT) is an important tool to produce these advanced polymers with also a low PDI. Therefor, this research focuses on the introduction of AMPS as embedded anion to the backbone of a solid polymer electrolyte containing Li^+. The hard/hydrophobic part of this polymer is containing styrene and the grafted hydrophilic part to be PEO, similar to other reports. [27, 24, 25, 29] The molecular weight is also found to be important to the ionic conductivity, so the same DP of Beaudoin et al. [24] was taken as inspiration for the size of the polymer.

An important part of this investigation is to determine whether the produced triblock brush-copolymers are able to function as a solid polymer electrolyte (SPE) in a lithium battery. The standard procedure for electrochemical tests is performed on a so called electrochemical impedance spectrometer. With this device it is possible to determine the resistance and with that the ion conductivity of the polymers when applied as electrolyte. Next, cycleability is also a desired factor in batteries, since solid polymer electrolyte species tend to degrade over the periods of charge-discharge cycles. In this part key segments for characterization of a solid polymer electrolyte (SPE) will be highlighted and explained.

1.7 Electrochemical impedance spectroscopy (EIS)

By introducing an alternating current to the specimen with varying frequency, the response in the form of magnitude and phase-shift is determined. [30, 31] This is the general theory describing impedance spectroscopy. When discussing an electrolyte it is important to look for the resistance of the species. Resistance, in the form of an electrolyte, directly translates to the ionic conductivity. Impedance is best described as seen in formula 1 where the input signal is described as E(t), as can be seen in formula 2, where E(t) is the peak voltage amplitude, ω is the angular frequency and t is the time. The resulting current, j(t) shares the same frequency as the input but can differ in phase and magnitude. The output signal is defined by formula 3 where j(t) is the output peak current density, $|j\Delta|$ is the amplitude of the current density and $(\omega + \Delta t)$ is the phase angle, also ϕ.

$$Z(t) = \frac{E(t)}{j(t)} \tag{1}$$

$$E(t) = |\Delta E(t)|sin(\omega t) \tag{2}$$

$$j(t) = |\Delta j(t)|sin(\omega t + \Delta t) \tag{3}$$

Because impedance is determined by phase and magnitude shift, its resulting signal can be represented in a Real and Imaginary component. The impedance $|Z(t)|$ can be described in the Real component $Re(Z)$ or Z' and in the Imaginary component $Im(Z)$ or Z''. In EIS the frequency of the signal is changed to investigate different interactions occurring on different frequencies. For instance, the mobility of ions is generally found

on the higher frequencies. [30, 32, 31] When defining the impedance at different frequencies, formula 4 can be used which describes the general output of the EIS.

$$|Z(\omega)| = \sqrt{Re(Z(\omega))^2 + Im(Z(\omega))^2} \tag{4}$$

When plotting EIS data containing magnitude and phase change on a trigonometric expression, generally Nyquist or Bode plots are used. In the case for simplicity, Nyquist plots (figure 8a) are preferred. Here, the phase angle (ϕ) is the angle from the origin and the magnitude the length of the vector. ϕ can be expressed as the inverse tangent of the Real component over the Imaginary, as seen in formula 5.

$$\phi(\omega) = tan^{-1}\frac{Re(Z(\omega))}{Im(Z(\omega))} \tag{5}$$

When modelling an electrolyte, first the theoretical equivalent circuit needs to be determined in order to find data corresponding to an electrolyte, theory on these equivalent circuit elements can be found in *Electrochemical Impedance Spectroscopy* written by Orazem and Tribollet. [31] Equivalent circuits are a way of expressing certain elements of the spectrum.[31] As mentioned, electrolytes behave as resistors since its purpose is to conduct charge in the form of ions. When measuring the impedance, the conduction of ions are only held up by the electrolyte. The presence of a capacitor (C_1) in the equivalent circuit is mathematically needed for model purposes.

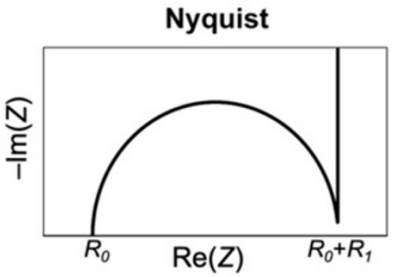

(a) Example of a Nyquist plot.

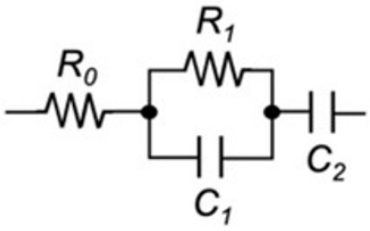

(b) A resistor circuit element used as the equivalent circuit for modelling an electrolyte.

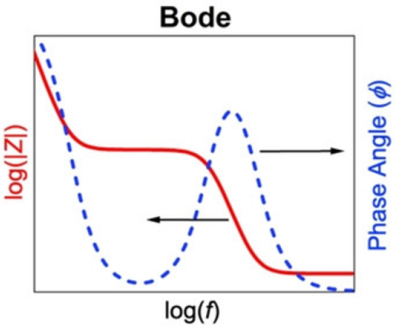

(c) A schematic illustration of a Bode plot of EIS.

Figure 8: An example of a result obtained from EIS. The semi-circle of the Nyquist plot is visible and also the points of R_0 and $R_0 + R_1$ which corresponds to the resistances of the tested specimen. Figure 8c shows an example of a Bode Figure 8b shows the circuit element where the analysis is based on, in accordance with Orazem and Tribollet. [31] The figures are obtained from [30].

An ideal resistor does not undergo a phase shift compared to the input signal. [30] For this reason, an ideal resistor does not have an Imaginary component and with that, the influence of the capacitor goes to zero, as is obtained from formula 7.

$$Z_R = R \tag{6}$$

$$Z_C = \frac{-j}{\omega C} \tag{7}$$

When dealing with an ideal resistor, the impedance is equal to the resistance and also no phase shift, meaning; when looking at a Nyquist plot, the resistance can be found at (or near) the x-axis (where the Imaginary component is 0). In other words, when looking at a Nyquist plot (figure 8a) a semi circle can be drawn and the places where the semi-circle intersects the x-axis, the resistance of a certain element is found. When looking at the equivalent circuit, R_0 is the place where the resistance of the phase before the electrolyte (for instance the electrode) is depicted, also seen in the Nyquist plot as R_0. R_1 is the resistance of interest since this is the one connected to the resistance of the electrolyte. [30, 31] On a Bode-plot (figure 8c), this point is shown at the place where the phase shift is zero, or when the graph of the *phase angle* is flat, the maximum resistance is found at the impedance at that point.

$$\sigma_{ion} = \frac{l}{R_{total} A} \tag{8}$$

To convert the resistance of the tested specimen to the ionic conductivity of the assigned polymer, the resistance found in the measurements are implemented in formula 8. Here, σ_{ion} is the ionic conductivity (S/cm), l is the thickness of the membrane (cm), R_{total} is the total resistance of the membrane (Ω) and A is the area (cm^2). The conductivity is temperature dependant, so the EIS measurements are taken above the Glass transition temperature (T_g) with a number of increments in temperature. By plotting the logarithm of the ionic conductivity on the inverse of temperature, a linear relationship becomes visible, as can be seen in figure 9. The linear fit to this plot is found in the Arrhenius conductivity relationship, formula 9. This linear relationship gives the activation energy (E_A) of the solid polymer electrolyte.

$$\sigma_{ion}(T) = \sigma_0 exp(-\frac{E_A}{RT}) \tag{9}$$

Formula 9 shows the Arrhenius conductivity equation where σ_{ion} is the ionic conductivity (S/cm) σ_0 is the pre-exponential factor (S/cm), E_A is the activation energy (kJ/mole), R is the universal gas law ($8.314\,\mathrm{J\,mol^{-1}\,K^{-1}}$) and T the temperature (K).

1.7.1 Cyclability tests

Charging and discharging of a battery influences the stability of the electrolyte, moreover, the heat-generation associated with this cycle also influences the SPE. This influence can be measured by EIS through cycling the scan multiple times to see whether the resistance increases. Multiple papers report loss in conductivity after cycling the electrolyte numerous times. [6, 13, 28]

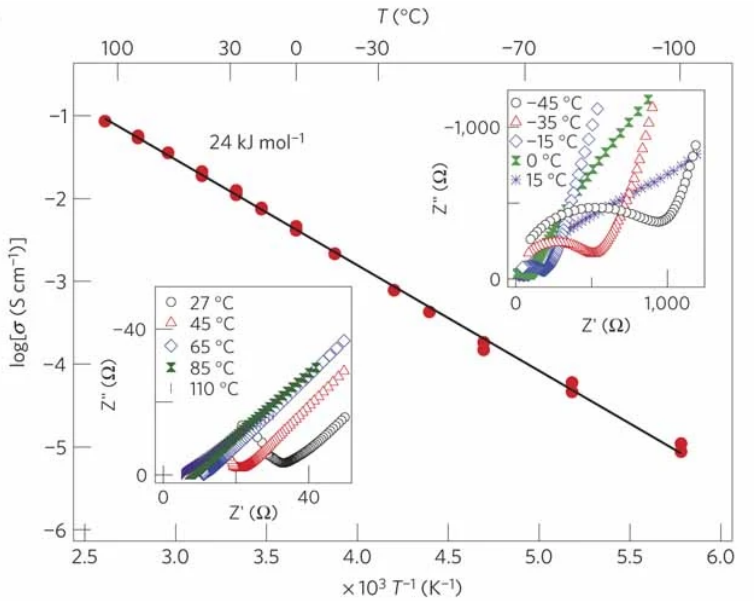

Figure 9: An example of an Arrhenius plot from a solid electrolyte. The linear fit of the line can be used to determine the activation energy of the electrolyte according to formula 9. Figure is used from [33].

1.7.2 Electrochemical impedance spectroscopy on solid polymer electrolytes

In order to understand how the ionic conductivity relates to other solid polymer electrolytes of similar characteristics, results of Bouchet et al. [25, 29], Sadoway et al. [23] and Bates et al. [27] were used for comparison since the polymers they produced also contained the anionic part embedded to the polymer chain. Also the research done by Beaudoin et al. [24] was used to investigate the influence of adding anionic parts to the polymer.

2 Experimental

2.1 Materials

Styrene, PEGMA, AMPS, Et_3N, ACVA were purchased from Sigma-Aldrich. PEGMA was purified through an Alumina-Oxide column before polymerization. DMAcTTC was synthesized using the method of Liang et al. [34] and obtained from previous experiments of Guzik et al. [35] 1,4-Dioxane, Deuterated Chloroform ($CDCl_3$), Deuterated Dimethylsulfoxide (DMSO-d_6), HPLC grade ($\geq$99.9%, inhibitor-free) Tetrahydrofuran (THF) were also purchased from Sigma-Aldrich.

2.2 RAFT-polymerization

2.2.1 MacroCTA

The polystyrene-macroCTA is synthesized with the predicted molecular weight based on formula 10. Here the targeted molecular weight ($M_{n,th}$) is determined by the concentration of the monomer $[M]_0$, the molecular weight of the monomer M_M, the concentration of the CTA ($[CTA]_0$) and the mass of the CTA (M_{CTA}). As mentioned in section 1.5 the targeted molecular weight of the macroCTA is based on the work done by Perrier.[18] The molecular weight is targeted at 7100 g/mol where the RAFT agent is active on both ends, meaning the polymer would propagate from the middle.

$$M_{n,th} = \frac{[M]_0 p M_M}{[CTA]_0} + M_{CTA} \tag{10}$$

In the initial calculations the assumed conversion was set at 60%, therefor a surplus of reactants would be needed. (208.5 mg 0.74 mmol) DMAcTTC, (41.9 mg 0,20 mmol) ACVA was put in a 25 mL round-bottomed-flask together with a neodymium stirring egg. Next, the flask was capped with a septum and placed under argon flushing. 15 mL of styrene was added in a flask and capped with a septum and flushed with argon for 15 min in order to remove potential present oxygen inside the liquid. 10 mL of 1,4-dioxane was put under the same treatment as styrene to remove the oxygen. Then, (9.2 mL, 0.08 mol) of argon-flushed styrene together with 4.3 mL of argon-flushed 1,4-dioxane was transfer to the 25 mL round bottomed flask under argon atmosphere. The system was flushed with argon for 15 minutes and a sample for ^{1}H-NMR analysis was taken before placing it into an oil-bath at a temperature of 80 °C. The reaction mixture was reacted for 45h after it was determined that at least 40% conversion was achieved, this was determined by ^{1}H-NMR analysis on a Bruker 400 MHz using d_6-DMSO as solvent for both before and after reaction. Flakes of solid material were visible within the reaction mixture. The round bottomed flask was cooled down to RT before the septum was removed. The reaction mixture was poured into 200 mL of methanol to precipitate the macroCTA. White flakes with a neon-yellow stain were visible in the mixture. The remaining solid was decanted from the liquid and washed a second time with methanol. The remaining wet solid was placed inside a vacuum oven at RT overnight after which the left over solid was collected (4.62 grams). 30.3 mg of solid, dried product was dissolved in 0.9 mL of $CDCl_3$ and measured in a 400 MHz Bruker ^{1}H-NMR. 15.4 mg

of product was dissolved in HPLC grade (≥99.9%, inhibitor-free) THF with three drops of technical grade toluene added. This sample was then analyzed on SEC with a GPC-column on a polystyrene standard. The determined molecular weight would be used in the conversion plots for the chain extension.

2.3 chain-extension

The target DP of the soft middle block is 208 based on the aforementioned sources. This is per polymer converted to the molar weight and with that the necessary components are calculated by using formula 10 assuming 100% conversion. The obtained polymers and its molecular weights can be found in table 1. The desired yield was 5 grams per polymer in order to have enough product for characterization.

2.3.1 Chain extension with PEGMA (RG17)

The first chain extension was performed with only PEGMA. (180.0 mg, 0.06396 mmol) of the PSt-macroCTA was added in a 15 mL scintillation vial together with (2.9 mg, 0.01 mmol) of ACVA. The vial is then capped with a rubber septum and placed under argon atmosphere. Then, 10 mL of PEGMA is run through a aluminium-oxide column in order to remove the inhibitor. The collected PEGMA is then put in a vial and capped with a rubber septum and placed under argon atmosphere to remove oxidative components from the reactant. A small amount of sample was taken from the reaction mixture for ^{1}H-NMR analysis in 0.9 mL $CDCl_3$. The reaction was then initiated by placing the vial in a 80 °C hot oil-bath and stirred vigorously. After 24 hours of reacting, the vial was raised out of the oil-bath and cooled down. When the reaction mixture reached room temperature, the rubber septum was removed. The content of the vial was transferred to a screw-cap tube filled with milliQ water and shaken vigorously. The polymers clearly swelled to form a hydro-gel. The formed product was transfered to a 8000 Da MWCO(molecular weight cut-off) to perform dialysis on the polymer with milliQ being the mobile phase. An ^{1}H-NMR of the dialysis liquid showed that there was PEGMA present in the liquid, but no arene peaks were visible, reassuring that there was no product leaking through the pores.

Table 1: The targeted composition of the polymers where degree of polymerization (DP) is given for the amount of monomers within the chain. The first two letters of the tag for the polymers are the initials of the author.

Tag	DP				Ratio	
	Styrene	PEGMA	AMPS	$M_{n,th}$ (g/mol)	PEGMA:AMPS (%:%)	[EO]:[Li]
RG17	54	208	0	109624.1	100:0	1:0
RGA	54	167	41	97445.3	80:20	32:1
RGB	54	146	62	91355.9	70:30	19:1
RGC	54	187	21	103534.7	90:10	71:1
RGD	54	104	104	79177.1	50:50	8:1

2.3.2 Chain extension with PEGMA and AMPS (RGA-D)

80:20 PEGMA:AMPS chain extension (RGA)

After the chain extension with PEGMA was determined to be a succes, the next step was to add AMPS to the polymer backbone. The molecular weight of the monomer was the weighed average of both monomers by ratio according to formula 11 where x_i is the fraction of monomer and M_i the molar mass of the assigned monomer. The 80:20 ratio is based on percentage of PEGMA and AMPS present in the middle block of the triblock. The DP is retained for every polymer synthesized, so in this case the targeted $M_{n,th}$ is 97445.3 g/mol.

$$M_M = \sum_{i=1}^{N} (x_i M_i) \tag{11}$$

For this, (403.3 mg, 0.072 mmol) PSt-macroCTA together with (4.6 mg, 0.014 mmol) ACVA were added to a 15 mL scintillation vial capped of with a rubber septum in order to put the content on an argon atmosphere. Another vial was prepared with (0.619 mg, 2.99 mmol) AMPS and (0.47 mL, 3.37 mmol) Et_3N to perform neutralization of the AMPS similar to the experiment performed by Guzik et al. [35] 1 mL of 1,4-dioxane prepared by flushing it with argon was added to the AMPS and Et_3N mix. PEGMA was again prepared by rinsing it through an aluminium-oxide column to remove the inhibitor. 10 mL of PEGMA was extracted via this method and rinsed with argon. The prepared AMPS mix together with (5.93 mL, 0.0120 mol) PEGMA from the prepared vial were added to the macroCTA and initiator mix. This reaction mixture was flushed another 15 minutes before a sample for ^{1}H-NMR was taken (dissolved in 0.9 mL $CDCl_3$). The reaction was started by lowering the vial into an oil-bath at 80 °C and stirred vigorously. Samples were taken after 30, 60, 120, 240, 360 and 1440 minutes used to determine the conversion over time and to find the kinetics which is explained in section 3.1.2. The method to exchange the protonated Et_3N with lithium ion is described in section 2.3.3. The preparation of all the other polymers followed a similar fashion with different amounts of the components. These amounts can be found in table 2.

Table 2: The targeted amounts of components needed for the initial reaction as described in chapter 2

		mL added	(g) added	mole
RG17	AMPS	0,000	0,000	0,000E+00
	PEGMA	4,725	5,198	1,040E-02
	ACVA	2,80E-03	2,80E-03	9,990E-06
	DIOX	3,049	3,140	3,564E-02
	MacroCTA	0,403	0,403	6,953E-05
RGA	AMPS	0,563	0,619	2,987E-03
	PEGMA	5,929	6,522	1,304E-02
	ACVA	4,03E-03	4,03E-03	1,438E-05
	DIOX	3,05	3,142	3,565E-02
	MacroCTA	4,02E-01	0,40228	6,936E-05
	Et3N	0,47	0,341	3,372E-03
RGB	AMPS	0,564	0,991	4,782E-03
	PEGMA	5,534	6,087	1,217E-02
	ACVA	4,30E-03	4,30E-03	1,534E-05
	DIOX	3,05	3,142	3,565E-02
	MacroCTA	4,29E-01	0,42909	7,398E-05
	Et3N	0,667	0,484	4,785E-03
RGC	AMPS	0,564	0,291	1,404E-03
	PEGMA	6,278	6,906	1,381E-02
	ACVA	3,79E-03	3,79E-03	1,352E-05
	DIOX	3,052	3,144	3,568E-02
	MacroCTA	3,79E-01	3,79E-01	6,528E-05
	Et3N	0,196	0,142	1,406E-03
RGD	AMPS	0,564	1,905	9,192E-03
	PEGMA	4,561	5,017	1,003E-02
	ACVA	4,96E-03	4,96E-03	1,770E-05
	DIOX	3,039	3,130	3,553E-02
	MacroCTA	4,95E-01	4,95E-01	8,536E-05
	Et3N	1,3	0,944	9,327E-03

2.3.3 Ion-exchange

The following step was to exchange the protonated Et_3N with lithium ions. The theory is similar to the method used by Guzik et al. [35] where through an acid-base reaction the protonated Et_3N gets converted into gaseous Et_3N, water and the lithium cation adding to the anionic AMPS. This is done by adding LiOH which will reduce the Et_3N after which the deprotonated Et_3N becomes immiscible and leaves the reaction mixture. This reaction can be seen in figure 2.3.3. The following step was to try using the same membrane sack used for dialysis after the chain-extension reaction. The membrane filled with polymer would be transferred to a milliQ water solution where a pH-sensor was added to as well. An enclosed system was erected where, through a septum and a small air-tight hole, the pH-sensor and the 0.1M LiOH would be added. The used set-up can be seen in figure 16 on page 36. For the titration of 0.1M LiOH on the polymers containing protonated Et_3N a pH-sensor was used. This was a WTW inoLab pH 730 with a SenTix 81 electrode. The sensor was calibrated on a 7.00 and 10.00 buffer solution.

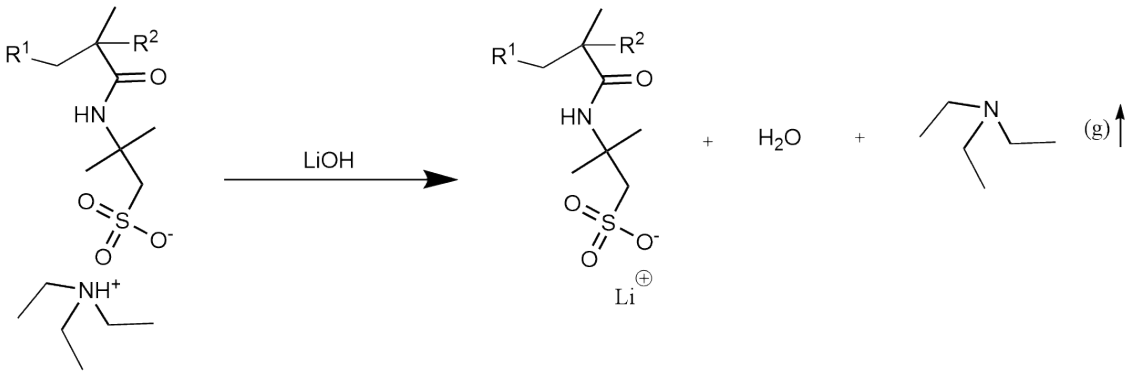

Figure 10: The cationic exchange of protonated Et_3N with ionic lithium

2.4 Characterization

Proton nuclear magnetic resonance

^{1}H-NMR is used to determine the conversion of the monomers, determining the ion-exchange conversion and the characterization of the end product. $CDCl_3$ was used as solvent for all the ^{1}H-NMR analyses. For the measurements a Varian MERCURYplus 400 MHz and a Bruker 600 MHz have been used. 30 mg/ml is chosen as the concentration for the measurements, because this gave the most accurate spectra.

Carbon-13 NMR (^{13}C-NMR), Diffusion ordered spectroscopy (DOSY), Quick, quantitative hetero-nuclear correlation (QQ-HSQC)

^{13}C-NMR, DOSY and QQ-HSQC were performed on a 600 MHz Bruker with $CDCl_3$ as solvent. QQ-HSQC was performed according the method described by Peterson et. al [36], and Hu et al. [37, 38].

Thermogravimetric analysis

Thermogravimetric analysis (TGA) is mainly performed to determine the decomposition temperature for determining the DSC temperature range (described in section 'Differential scanning calorimetry'). The analyses were performed on a PerkinElmer TGA-4000 with the temperature range set at ambient to 400 °C.

Differential scanning calorimetry

The Differential scanning calorimetry (DSC) is used to proof the theoretical T_g of the polymer described by numerous of researches. [6] It was based on these papers that a Heat-Cool-Heat cycle is needed from −90 °C as minimum to a maximum of 110 °C. These analyses were performed on a TAinstruments DSC25 with a hermetic lid.

Gel Permeation Chromatography

GPC is performed on the PSt-macroCTA where 15 mg of product is dissolved in HPLC graded THF with 3 drops of toluene. The column used is a Hewlett Packard 1100 Series HPLC equipped with a GBC 1240 Refractive Index Detector (RID). Flow of 1 ml/min at 40°C using 3× Agilent Technologies PLgel Mixed E columns (300 × 7.5 mm 3µm Particle Size). With an injection volume of 20 µl and a Polystyrene calibration. Analyses on the extended polymers was impossible due to the end products being unable to dissolve in the solvents that the columns run on in the institute.

CHNS elemental analysis (CHNS-analysis)

The composition of the end-products is also measured via elemental analysis using an Elementar VarioMICRO CHNS. Here, mass-fractions of carbon, hydrogen, nitrogen and sulfur are determined simultaneously. It is a convenient tool for indicating the amounts of these elements present within the sample and with that give an indication of the composition of the polymer. The predicted ratios of these elements provided to the lab technician was based on the predicted composition of monomers using a 100% conversion.

Inductively coupled plasma mass spectrometry

Inductively coupled plasma mass spectrometry (ICP-MS) is performed to determine the success of the ion-exchange experiment described in section 2.3.3. Here the mass-fraction of sulfur is measured to the mass-fraction of lithium. The tests are performed in duplicates.

Cell preparation

The polymers that were created were first freeze dried in order to remove any moisture potentially present within the sample. This could hinder the conductivity of ions due to the interactions. The dried samples were than transferred to a glove-box and set there for 12 hours to dry in that atmosphere before adding the samples to an EIS-cell. The polymers are measured for there size, rolled flat as much as possible before transfer to the cell. The tests were all performed in a Swagelok cell with a polyoxymethylene lining. It was air-sealed and contained no water. The frequency range was set between 1 MHz and 1 Hz with temperature steps ranging between 55 °C and 115 °C. The maximum temperature was based on the decomposition temperature found in the Thermogravimetric analysis (TGA), which is well below that number.

2.5 Scanning Electron Microscopy (SEM)

SEM imagery is for determining the supramolecular structure discussed in section 1.3. Several magnifications have been tried and also several samples have been taken. The magnification of interest was 2000x for RGB and 1000x for RGC. The analyses were performed on a Hitachi TM4000.

3 Results and discussion

3.1 Results

The goal was to synthesize triblock-copolymers with supramolecular structures based on phase separation. This was achieved by using DMAcTTC as RAFT-agent which propagate from the middle. The initiation and propagation for the chain extension happens also from the middle. In the first step it is important to know whether the synthesis of the macroCTA was successful since the same macroCTA was used for all the other polymers. The reaction scheme for the production of the macroCTA can also been seen in appendix A.6. For all the polymers, a handy oversight for the added components prior to the initiation can be found in table 4. The chain-extension was performed with different ratio of the monomers in order to produce polymers with different [EO]:[Li^+] ratio. Characterization of the polymers was difficult to determine the composition and size of the final products. This was mainly done using the conversion of the monomers by using ^{1}H-NMR.

3.1.1 MacroCTA

Based on formula 10, a targeted molecular weight could be determined by the added amount of reactants. These added components are listed in table 3 which translates into a molecular weight of $5500\,\mathrm{g\,mol^{-1}}$ with full conversion. The conversion was monitored using ^{1}H-NMR. This was done by integrating the peaks between 5.5 and 6.5 ppm, which are assigned to the alkene peaks, and the reference arene peaks between 6.5 and 7.5 ppm. This can also been seen in figure 11. By following the trend of this conversion, a kinetic plot can me made. This plot is found in appendix 29 on page 60 and it can be used to find the kinetic constant, which is found to be $3.17 \times 10^{-4}\,\mathrm{min^{-1}}$.

Table 3: The used amount of reactant for synthesizing the macroCTA.

Compound	mL	(g) added	Mole added
DMAcTTC	0.2078	0.2078	7.27E-04
ACVA	0.0419	0.0419	1.49E-04
Styrene	9.2	8.4	8.0E-02
Dioxane	4	4.12	4.68E-02

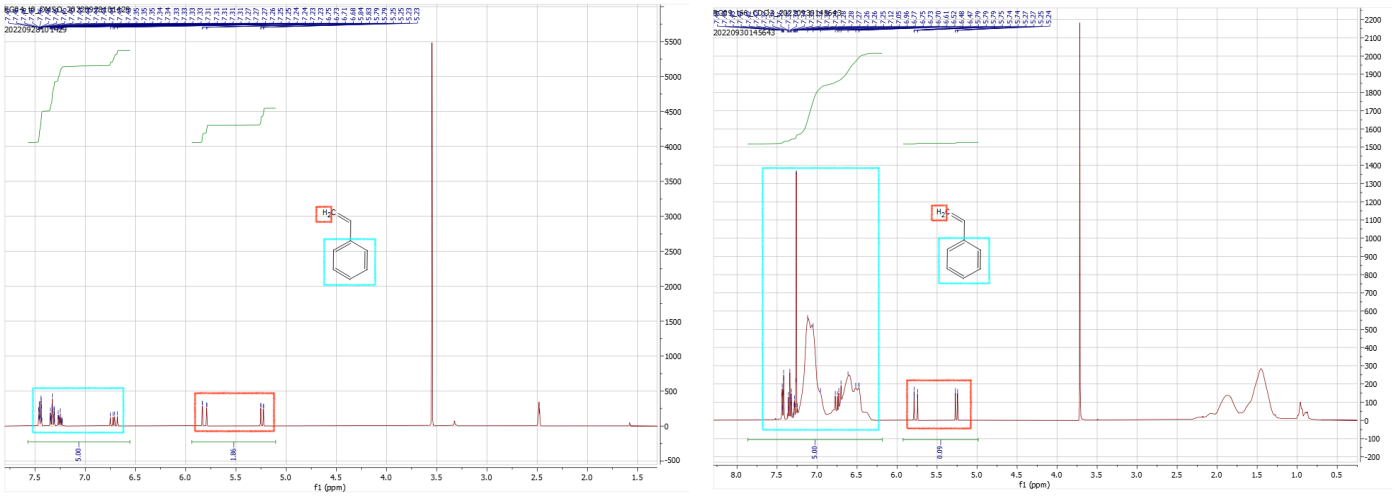

(a) The ^{1}H-NMR spectrum of the macroCTA at t=0 with the distinctive peaks between 5.5 and 6.0 ppm.

(b) Here the time is 66h after initiation and it can be seen that the

Figure 11: The used spectra of the macroCTA where the the peaks of interest are the alkene peaks between 5.5 and 6.5 ppm and the reference arene peaks between 6.5 and 7.5 ppm.

Determining the size of the macroCTA

Although the conversion of the monomers together with formula 10 would give an accurate indication of the molecular weight, it is important to test this theory by performing Gel Permeation Chromatography (GPC). The macroCTA was able to dissolve in THF, which meant that for this polymer GPC would be possible, more on that later. This, together with the size predicted by conversion and formula 10 would reassure the findings of the molecular weight. The GPC-data can be seen on figure 28 on page 60. Through this process it can be concluded that the molecular weight is $5800\,\mathrm{g\,mol^{-1}}$ which is close to the predicted molecular weight of $5500\,\mathrm{g\,mol^{-1}}$. The found molecular weight would translate to a structural formula of $\mathrm{PSt}_{27} - b - \mathrm{PSt}_{27}$ since the propagation happens from the middle. The DP of Polystyrene is useful later in the characterization of the chain extended polymers.

3.1.2 Chain extension with PEGMA (RG17)

Following the successfully synthesis and characterization, the production of the first chain extended polymer with PEGMA was tried. On the first hand, it was done to determine the success of propagating the macroCTA. Secondly, it was done to determine the characteristics of the longer polymer chain without AMPS present. And third, at this stage of the research, it was still investigated to add lithium salts to the polymer blend to potentially increase the ionic conductivity, however, it was understood that the addition of these lithium salts is complex and needs to happen in an inert environment because of their oxidative nature.[27] This was, unfortunately, not possible.

Synthesis

The amount of the necessary components were calculated using formula 10 where a DP for the middle block was set to be 208, so a DP of 104 PEGMA at both ends of the thiocarbonylthio group of the RAFT-agent. The added components to the mixture can be found in table 4. Due to a personal error, the conversion of this polymer was not measured, so the assumption is that there was full conversion. Also kinetics were not calculated because of this reason, but based on observations, conversion happened rapidly. The used components meant also diverting from the previous process in which methanol was used for purification, since Polystyrene would not dissolve in methanol, however styrene monomer would. Due to there being an overload of PEGMA within this polymer chain, it was uncertain whether this polymer would, in fact, dissolve in methanol. It was therefor decided to deviate to another purification method, namely dialysis. This method would also benefit the usage of components, namely less methanol, but also the ease in transfer of the dialysis membrane to the dialysis liquid and also to test the potential monomers present in there. Also, this approach would be beneficial for drying the polymer for end characterization.

Characterization

In order to understand the size and composition of the polymer, it is imperative to dissolve the polymer for characterization purpose. A complete solution of RG17 was not achieved by any present solvent. At this point it was not understood why, but more on that later. For this reason it became impossible to perform GPC since complete solution is needed. Furthermore, it was unsure whether a reliable ^{1}H-NMR spectrum could be obtained. Multiple solvents were tried here with $CDCl_3$ being the most useful since characterization would become possible. However, a clear spectrum could be obtained, the composition would become difficult. Therefore, the composition of the RG17 polymer was based on the DP obtained from the macroCTA together with the full conversion of all the added PEGMA. This resulted in a total DP of 333 for PEGMA, meaning a structural formula of $PSt_{27} - b - PEGMA_{333} - b - PSt_{27}$. This is a higher DP than anticipated and is attributed to a *beginners mistake* since this was the first time the chain extension was performed. Furthermore, the extra parts of PEGMA was thought to not hinder the further process.

3.1.3 Chain extension with AMPS and PEGMA (RGA-RGD)

After the chain-extension of the macroCTA with PEGMA was performed, another step was set in performing a chain-extension with AMPS and PEGMA. 1,4-dioxane was chosen as reaction solvent which was also used in the other reactions. AMPS is known to not dissolve in 1,4-dioxane on its own and also not to polymerize with lithium as counter-ion to the AMPS. [39] Another method was used in order to polymerize the AMPS, namely introducing Et_3N as counter-ion similar to how Guzik et al. performed this RAFT polymerization, as can be seen in figure 12. [35] This is in order to make the monomer less hydrophilic and therefor able to dissolve in organic solvents. In theory, an equimolar amount of Et_3N should be added, however, this was not the case for all the experiments based on observations of turning the crystalline solid into a liquid that would dissolve in 1,4-dioxane. This can easily been seen in table 4.

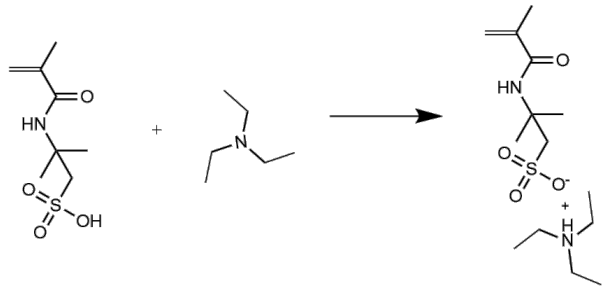

Figure 12: The step in which the AMPS monomer is prepared with adding Et_3N counterion.

The necessary amounts needed for the targeted DP and ration of PEGMA:AMPS was determined using formula's 10 and 11. The added component to the mixture can be seen in table 4 and using the same method as described in section 2.3.2. After the preparation of the monomers is completed, the next step of the polymerization was to take a sample for conversion. The conversion was monitored during the duration of the reaction by means of ^{1}H-NMR spectra using $CDCl_3$ as solvent. Samples were taken with surplus argon flusing in order to not let oxygen or water enter the reaction atmosphere and terminate the reaction. The reaction would continue for 24h after which the reaction would be terminated by cooling the mixture to room temperature as per normal procedure.

Characterization

As can be seen in figure 13 (page 30), the conversion was determined based on the integral of the alkene peaks between 5.4 and 6.2 ppm. In this figure the peaks are highlighted per molecule. The reference peaks are from the polystyrene which has, as discussed in section 3.1.1, the DP of the styrene is known and also its arene chemical shift is isolated from the other compounds, between 6.3 and 7.2 ppm. This means that the styrene peaks can be reliably used as reference for conversion of the alkene peaks of PEGMA and AMPS. The alkene peaks of both AMPS and PEGMA can be distinguished from on another by the fact that there are singlets for both compounds and one compound is more present than the other. PEGMA is in this case more present than AMPS. This theory is also tested by taking an ^{1}H-NMR of both compounds in $CDCl_3$.

The peaks would be deconvolved by using the peak fitting and hiding tool from MestreNova, which is tested to give an accurate result and would be more convenient. The resulting conversion can be determine by taking the integral of the alkene peaks at a certain time stamp and relate it to the integral at t0. The resulting conversion graphs can be found in appendix A.4 on page 62 with also the resulting $\boldsymbol{k}$-values and $t_{\frac{1}{2}}$ values. As can be seen there, 100% conversion was never reached and this is also taken into account later in the discussion of the results. Complete solubility of all the polymers remained a challenge throughout the characterization process. For this reason became GPC impossible hence the determining of the DP would be based on the conversion of the added monomers which is, based on the results for the macroCTA in section 3.1.1, accurate enough. Characterizing the polymer for composition based on the end-product would also be a hard task, because the peaks of both AMPS and PEGMA would both overlap at the same chemical shift. More on this in section 3.1.7.

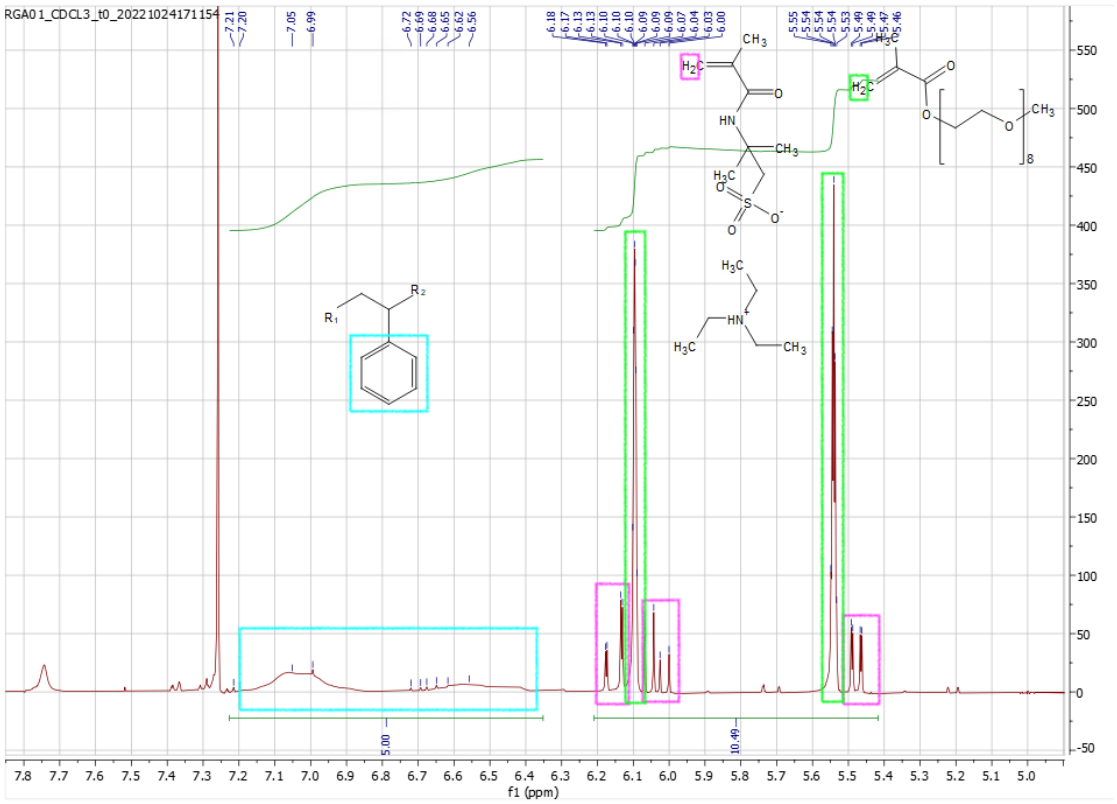

(a) Alkene peaks of the monomers seen at the start of the reaction.

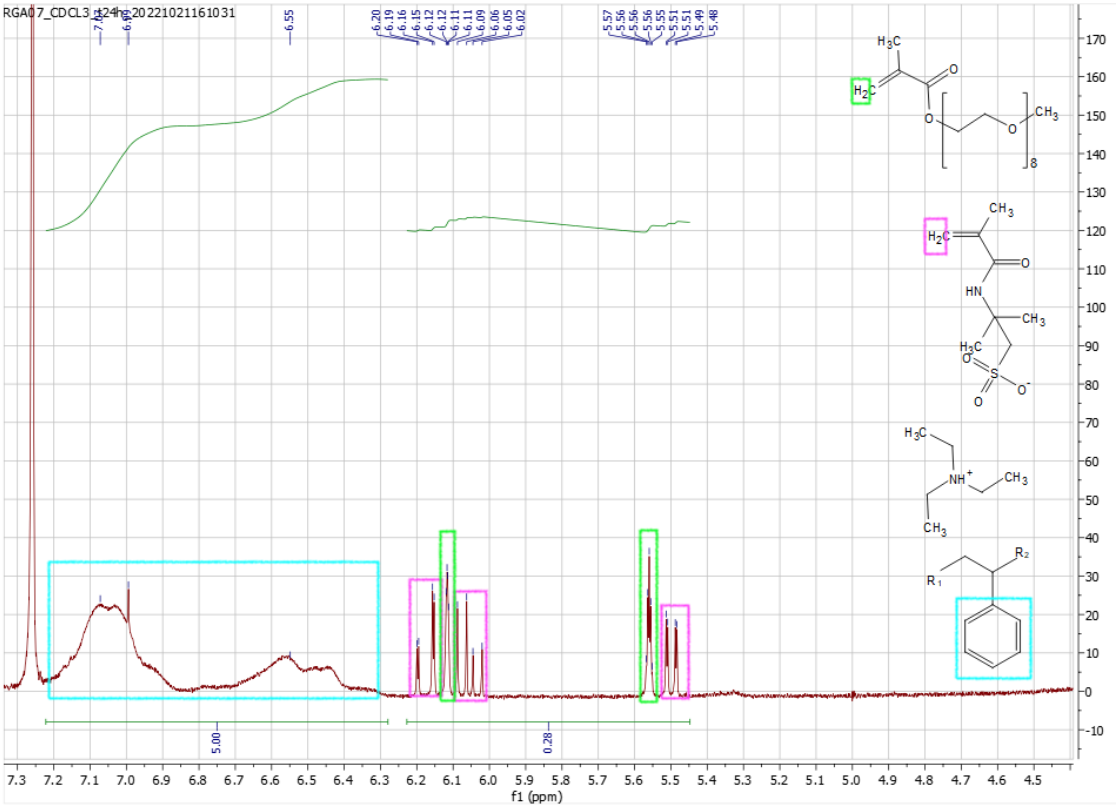

(b) Alkene peaks of the monomers seen at the end of the reaction after 24 hours and before the dialysis.

Figure 13: The used technique to determine the conversion of the monomers.

Table 4: The added components to the reaction mixture.

	Compound	(mL) added	(g) added	mole
RG17	AMPS	0.000	0.000	0.000E+00
	PEGMA	4.700	5.170	1.034E-02
	ACVA	2.80E-03	2.80E-03	9.990E-06
	DIOX	2.000	2.060	2.338E-02
	MacroCTA	0.180	0.180	3.103E-05
RGA	AMPS	0.564	0.6203	2.993E-03
	PEGMA	5.93	6.523	1.305E-02
	ACVA	4.06E-03	4.03E-03	1.438E-05
	DIOX	3	3.090	3.507E-02
	MacroCTA	4.03E-01	0.40228	6.936E-05
	Et3N	0.47	0.341	3.372E-03
RGB	AMPS	0.903	0.9928	4.791E-03
	PEGMA	5.54	6.094	1.219E-02
	ACVA	4.90E-03	4.90E-03	1.748E-05
	DIOX	3.05	3.142	3.565E-02
	MacroCTA	4.30E-01	4.30E-01	7.407E-05
	Et3N	0.95	0.690	6.816E-03
RGC	AMPS	0.265	0.291	1.404E-03
	PEGMA	6.278	6.906	1.381E-02
	ACVA	3.79E-03	3.79E-03	1.352E-05
	DIOX	3.1	3.193	3.624E-02
	MacroCTA	3.80E-01	3.80E-01	6.552E-05
	Et3N	0.45	0.327	3.229E-03
RGD	AMPS	1.732	1.905	9.192E-03
	PEGMA	4.56	5.016	1.003E-02
	ACVA	4.96E-03	4.96E-03	1.770E-05
	DIOX	3.3	3.399	3.858E-02
	MacroCTA	4.96E-01	4.96E-01	8.553E-05
	Et3N	3.3	2.396	2.368E-02

CHNS elemental analysis (CHNS-analysis)

A CHNS elemental analysis (CHNS-analysis) was performed on RGA in order to find the amounts of carbon, nitrogen, hydrogen and sulfur relative to one another and whether this would match with the amounts of monomers added. Sulfur and nitrogen are (mostly) assigned to AMPS, so the relative wt% would give an indication of the content of the polymers by the present sulfur and nitrogen assigned to the AMPS. This is by assuming good purification, so all the unreacted AMPS was removed. Table 5 and 6 show the method of prediction and the results of the CHNS-analysis.

Table 5: Based on the number of atoms assigned to the polymer, the wt% of the elements within the polymer chain can be calculated. This number will give an indication of the elements found in the polymer and will be compared to the results found in table 6.

Element	C	H	N	S	O
Total number elements based on DP	5242	9739	86	40	2196
RAFT agent	8	14	0	3	4
Total	5250	9753	86	43	2200
Elemental weight (g/mol)	12	1	14	32	16
Total contributing weight of element (g/mol)	63004.24	9752.87	1204.63	1389.33	35200.46
wt% of element	56.99	8.82	1.09	1.26	31.84

Table 6: Results of the CHNS-analysis performed by Ing. J. van der Velde on a Elementar VarioMICRO CHNS.

Results no.	Name	N (wt%)	C (wt%)	H (wt%)	S (wt%)
11	RGA12	0.69	56.29	8.65	0.75
12	RGA12	0.62	56.13	8.71	0.68

The results are overlapping with the predictions, however, the amount of nitrogen and sulfur is lower than expected. The predictions are based on the conversion of the added components and the total expected weight as a consequence. In this case there might be a few scenario's as to why this is the case; there is relatively less sulfur compared to the carbon in the measured result than the predicted results. This can because there is less AMPS within the polymer or too much PEGMA within the polymer, or the measurement is inaccurate. As can be seen in appendix A.5 in tables 15 and 16 where the predicted results are based on either twice the amount of PEGMA present in the reaction mixture or half of AMPS present in the reaction mixture. The relative lower amount of sulfur and nitrogen can be explained via this method. Extra PEGMA is of course not possible, so the other option where the conversion of AMPS is lower is the more realistic option. This contradicts, however, with the found conversion by the ^{1}H-NMR analysis discussed in section 3.1.3.

3.1.4 Ion exchange

In the next step, the AMPS-Et_3N segments (within the polymer chain) will be neutralized to form AMPS-Li segments. Several methods to achieve this have been proposed, like working with LiH to form H_2 in the process, as is for instance performed by Bates et al. [27] This method became very impractical due to several pieces of equipment not being present. The other method is, like already mentioned, based on the ion-exchange method similar to how Guzik et al. performed it. [35] In this case Et_3NH^+ will be converted by LiOH in to Et_3N and H_2O, as can be seen in figure 14.

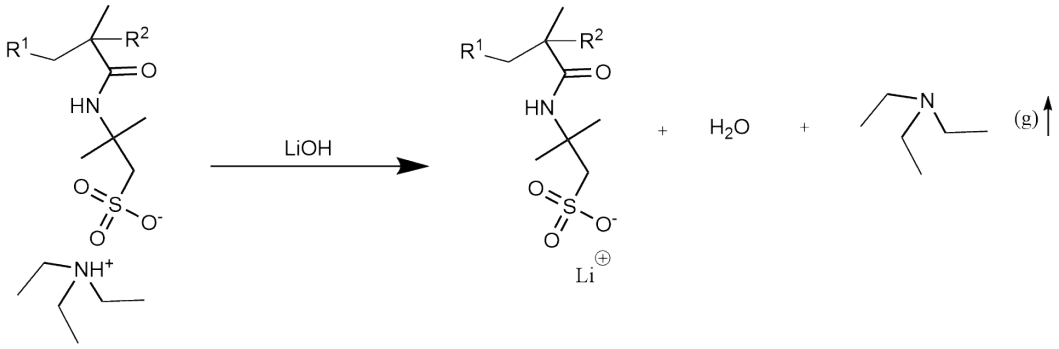

Figure 14: The cationic exchange of protonated Et_3N with ionic lithium

The ion exchange is performed in titration fashion where a 0.1M LiOH solution is added to the titration liquid. The polymer is contained within a dialysis membrane of 8000 MWCO as discussed in section 2.3.3. By adding the LiOH the Et_3NH^+ is converted in Et_3N and by increasing the temperature and also flushing the titration mix with argon, the Et_3N is forced out of the system, meaning there is no equilibrium. The set-up can be seen in figure 16a and the figure on the right (figure 16b) shows a pH-paper that was placed at the exhaust of the system were the Et_3N leaves the system. It is known that Et_3N has a pKa of 10.75, so an elevated pH was expected and also confirmed. [40] Added amounts of LiOH was monitored and can be seen in table 7 where the *'pH end'* is the pH noted at the point where there was no lowering in pH visible anymore, meaning no conversion of Et_3N anymore.

Table 7: The results of the titration for all the polymers with 0.1 M LiOH. Note that RGA is lower in the amounts of LiOH needed, this is because there was less (remaining) RGA used for this experiment.

	LiOH mL	pH start	pH end	mole LiOH unused	mole LiOH	mole AMPS	mole LiOH/mole AMPS
RGA	4.27	6.4	10.45	2.822E-04	1.45E-04	2.999E-04	0.48
RGB	31.3	7.6	10.83	2.512E-08	3.13E-03	3.990E-03	0.78
RGC	18.0	5.62	10.54	2.399E-06	1.80E-03	8.974E-04	2.00
RGD	47.0	6.13	10.82	7.413E-07	4.70E-03	8.186E-03	0.57

The set-up used a known amount of MQ-water (1.1 l) and a noted starting pH (as seen in table 7). Together with the end pH, a used amount of LiOH can be determined which directly translates into the amount of AMPS-Et_3NH^+ converted.

Other tested methods

Another method in the form of Karl-Fischer auto-titration with a Metrohn 848 Titrino plus was investigated as well. This was not successful because the reaction-speed happened too slow that the device detected equilibrium too soon. In fact, the reaction-speed was even slower than the absorption of CO_2. This was determine by testing a blank titration and see the response of the pH. With this information another set-up was created in the form seen in figure 16a.

Characterization

The presence of Et_3N within the polymer can easily been found on an ^{1}H-NMR spectrum by a distinctive triplet between 1.3 and 1.4 ppm, seen in figure 15. As seen in figure 15a this triplet is visible at the start of the titration. After the equilibrium of pH was found, the titration stopped and the polymer was dried, it was measured again by ^{1}H-NMR and, as is now visible, no triplet at that chemical shift present anymore. So, together with the pH and ^{1}H-NMR a fair assessment on whether the conversion was successful could be made.

Inductively coupled plasma mass spectrometry (ICP-MS)

A next step into determining whether lithium was present within the polymer, a Inductively coupled plasma mass spectrometry (ICP-MS) was performed. Before that, a prediction was made to understand the data and whether it is accurate.

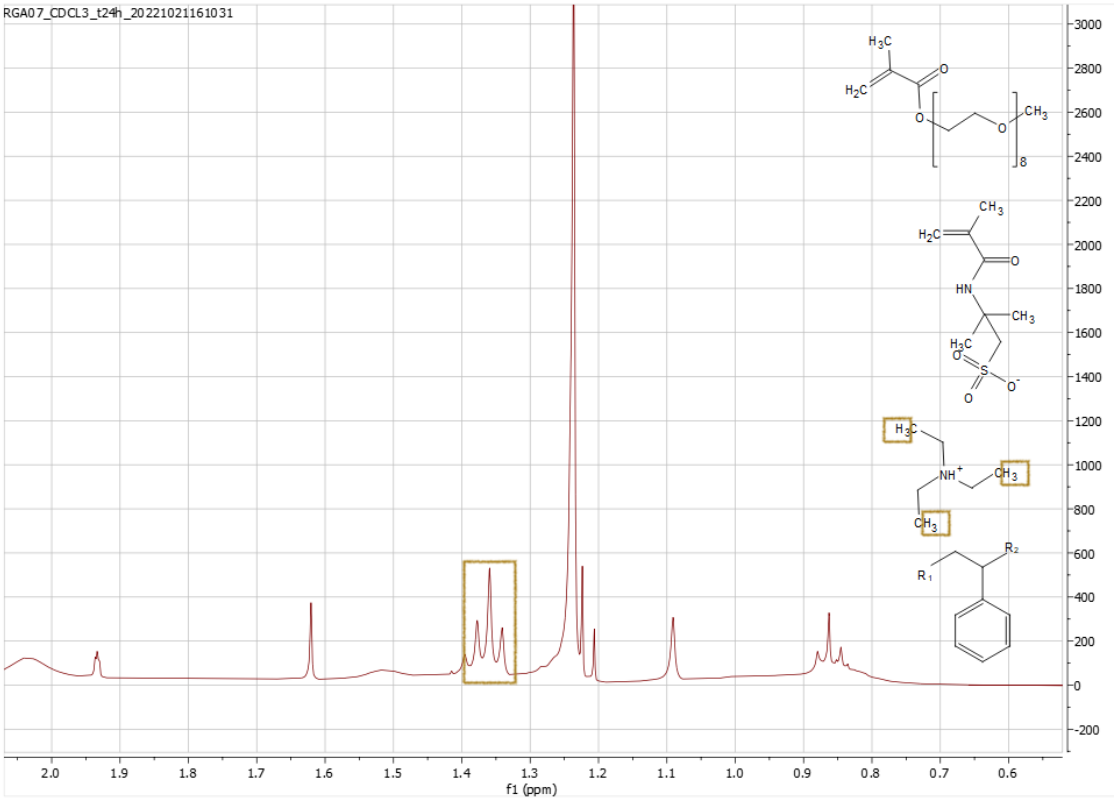

(a) Clear distinctive triplet of Et_3N

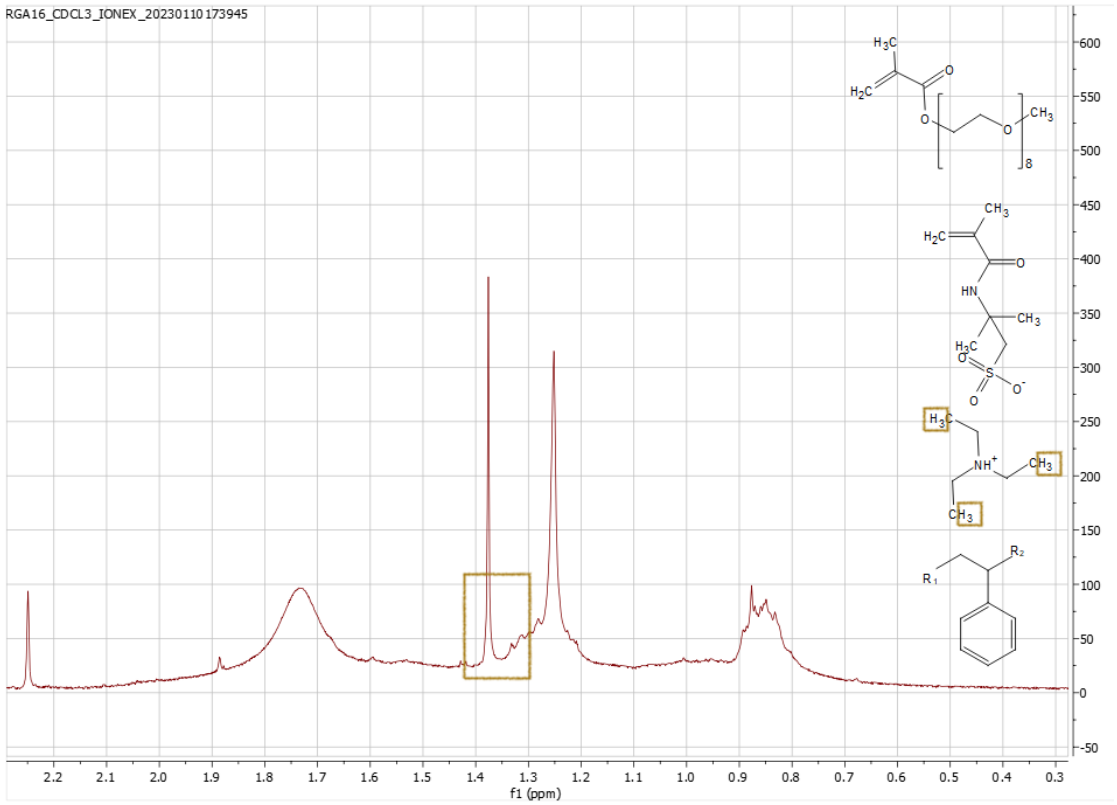

(b) There is no triplet visible anymore.

Figure 15: The monitored neutralization of Et_3N with the assigned peaks to the designated protons.

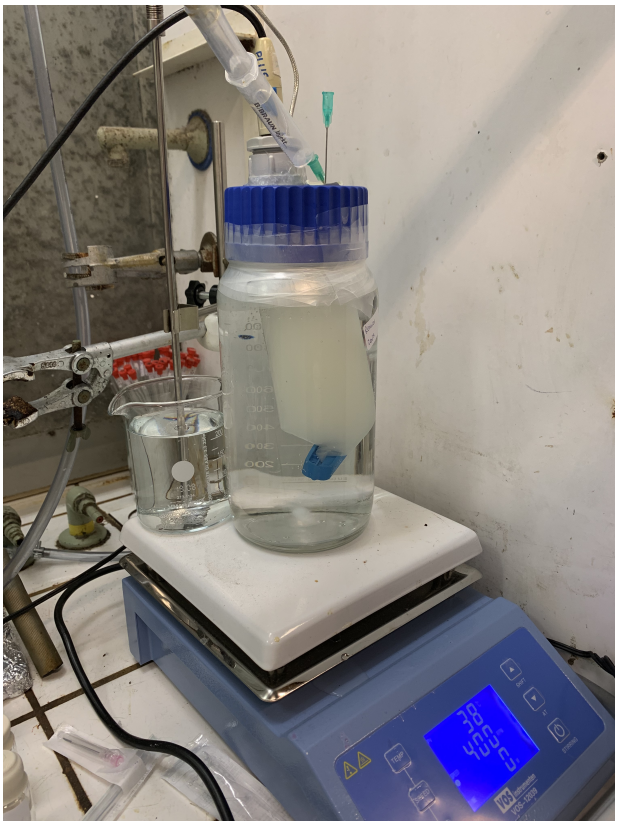

(a) The flask encapsulated with the membrane filled with the polymer inside.

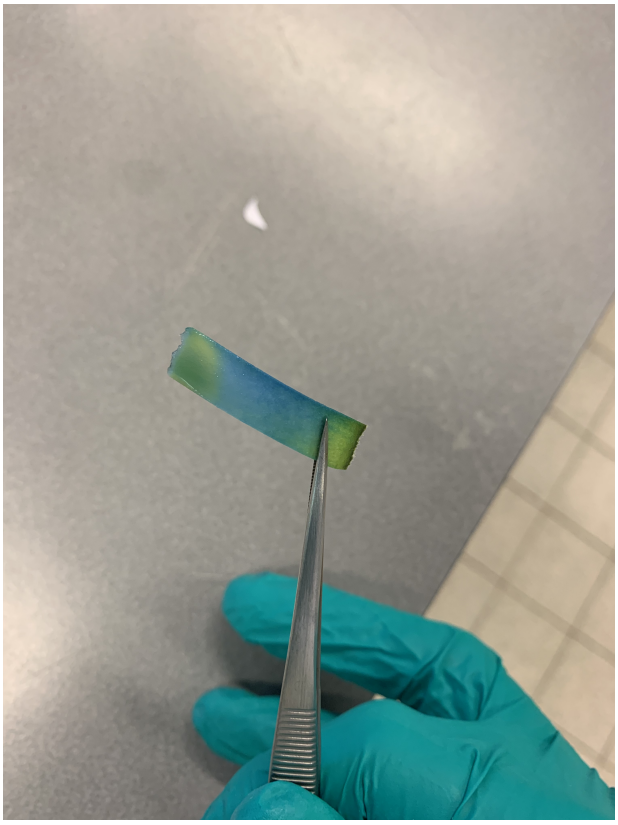

(b) pH-paper placed at the exhaust of the flask when flushed with argon. The pH-paper was sprinkled with MQ water before placing it at the exhaust.

Figure 16: Used set-up for the titration.

3.1.5 Inductively coupled plasma mass spectrometry (ICP-MS)

In order to confirm the presence of lithium within the polymer an other type of elemental analysis was necessary. For this, Inductively coupled plasma mass spectrometry (ICP-MS) became a viable option since it can measure both sulfur and lithium. The weight percentage of sulfur directly translates to the amount of AMPS present since it is mainly found in this part of the polymer chain. So, together with the wt% of lithium it is possible to determine the success of the ion-exchange.

Table 8: Results of the Inductively coupled plasma mass spectrometry (ICP-MS) analysis on all the polymers that underwent the ion exchange.

Sample code	Elements	AVG (m/m %)	STD (%)
RGA	Li	0.14%	0.01%
	S	0.88%	0.04%
RGB	Li	0.28%	0.00%
	S	1.63%	0.01%
RGC	Li	0.10%	0.02%
	S	0.36%	0.00%
RGD	Li	0.42%	0.00%
	S	2.95%	0.11%

On figure 17 the graph of the predicted ratio between lithium and sulfur is compared to the results of the ICP-MS, or the predicted ratio between OH^-, and with that Li^+, and sulfur compared with the results of the ICP-MS. The prediction are obtained via different methods; the theoretical (or targeted) ratio is determined by the full conversion of added components with equimolar LiOH, the *Conversion with equimolar LiOH* is based on the determined conversion of monomer components and equimolar titration of LiOH, the *conversion with titration data* is based on the amount of LiOH added minus the unreacted LiOH based on the pH. The x-axis is the ratio between AMPS and PEGMA where the theoretical number is based on the desired ratio, the other data points are based on the ratio determined by the conversion. When comparing the results of the ICP-MS with the predictions, it becomes clear that the trend of the data based on the titration overlaps. Note that this number is also based on an optimal transfer of product from the polymerization flask to the membrane.

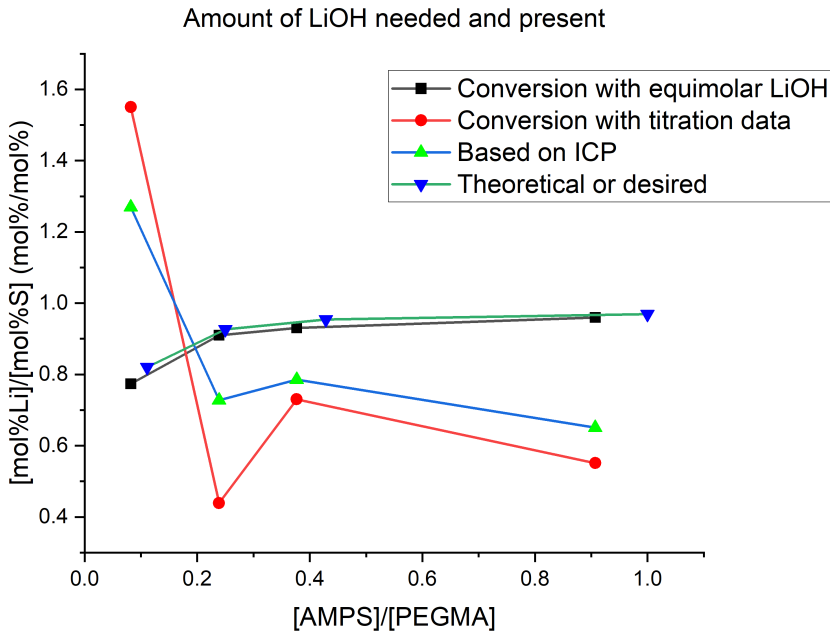

Figure 17: Predicted and determined $\frac{mol\%_{Li+}}{mol\%_S}$ as a function of $\frac{[AMPS]}{[PEGMA]}$

As can be seen in the figure above, the predicted wt% of lithium compared to the wt% of sulfur is similar to the predicted weight-percentages from the known amount of added LiOH and the conversion of the monomers. This data can then be translated into the [EO]:[Li^+] ratio as seen in table 9.

Table 9: The resulting [EO]:[Li^+] ratio based on the ICP-MS and conversion of monomer results.

	Actual [EO] : [Li^+]	Targeted [EO] : [Li^+]
RGA	50.26 : 1	32 : 1
RGB	29.51 : 1	19 : 1
RGC	83.82 : 1	72 : 1
RGD	14.79 : 1	8 : 1

These ratio's are important for evaluating the conductivity based on these ratio's later in section 3.3.1. It is clear that the targeted ratio's are not matched. This can be attributed to structural interference to the ion-exchange due to the polymer not able to fully dissolve in water, which was until then not considered as an issue since conversion was detected by pH-sensor and pH-paper at the exhaust and was found to be satisfactory at that time.

3.1.6 Diffusion ordered spectroscopy (DOSY)

Diffusion ordered spectroscopy (DOSY) was used in order to confirm that the polymerization occurred on the macroCTA, so diffusion on around the same number and with that on the same polymer strain.

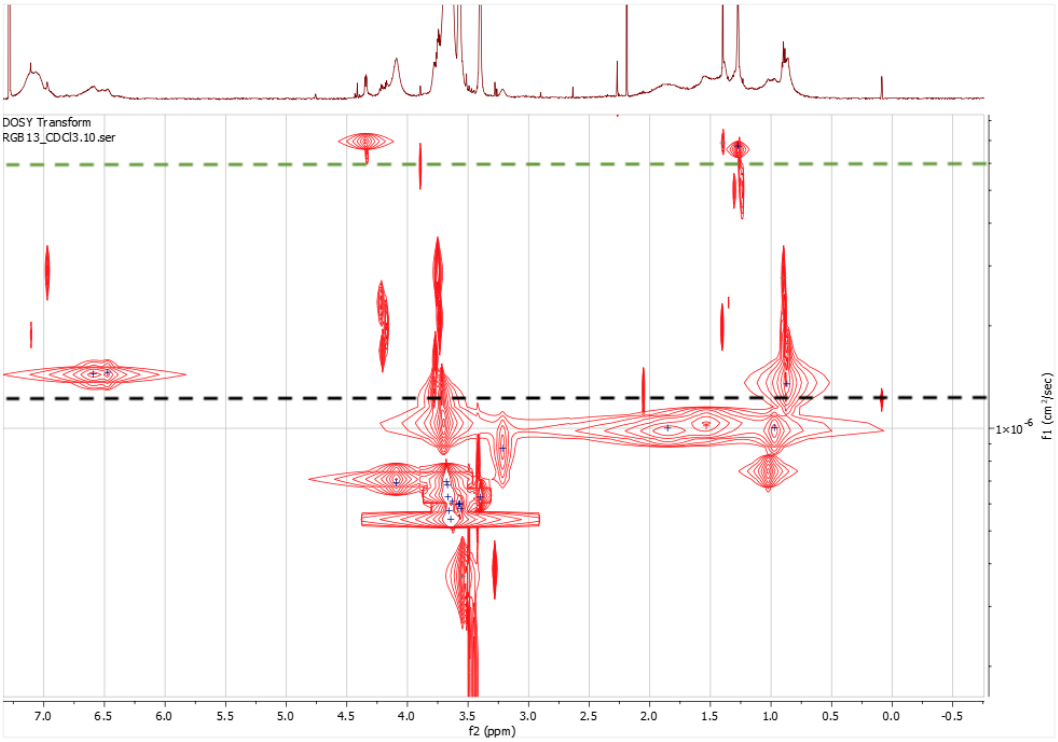

Figure 18: The DOSY spectrum of RGB as an example.

As can be seen in figure 18 the signals of the majority of compounds revolve around the same diffusion, meaning the polymerization happend on the same chain. This cannot tell something about M_w and with that also not about the PDI. However, this does give an indication that the chain extension of the macroCTA was successfully performed. The broad signal at 3.5 ppm is, according to Vièville et al, due to a higher PDI on solely the PEGMA block. [41] This could, however, not be tested on GPC. In this spectrum other signals are also visible. These are thought to be solvents, unreacted monomers and Et_3N since the diffusion is higher for these signal, meaning lower molecular weight.

3.1.7 Carbon-13 NMR (^{13}C-NMR) and Quick, quantitative hetero-nuclear correlation (QQ-HSQC)

Carbon-13 NMR (^{13}C-NMR) was tried because there was a lot of overlap visible in the ^{1}H-NMR spectra and it was tried, also with QQ-HSQC, to deconvolute the found spectra. ^{13}C-NMR was difficult, because an insufficient concentration was reached to find an aligning spectra. QQ-HSQC is quantitative tool in contrary to conventional HSQC. The QQ-HSQC works by combining four different INEPT delays into one spectrum. [36] The procedure of Peterson et al. is used to determine the number of certain C-H couplings within the polymer with the styrene blocks as the reference. Figure 19 shows the resulting extrapolated QQ-HSQC spectra where the logarithm of the integrals was taken and linearized to extrapolate towards $HSQC_0$. [37] As mentioned, the known concentration is the styrene block, since it is then known what the ratio would be between styrene and the other monomers. Table 17 shows the resulting integrals of the measurement. Although in the beginning stages this procedure looked promising, the accuracy of this method was determined to be insufficient. The error margin was too big, which resulted in not obtaining relevant data.

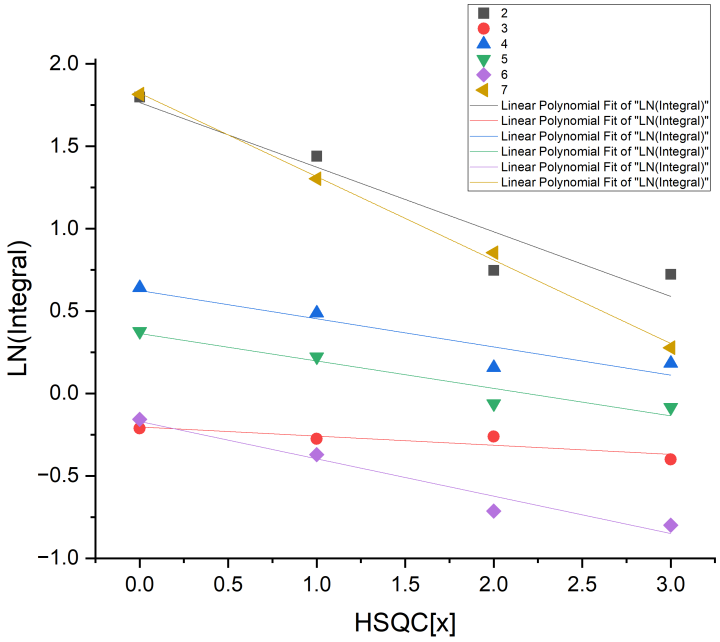

Figure 19: Result of the QQ-HSQC.

3.2 Physical property analysis

After the structural identity was confirmed, the next step was to find the mechanical characteristics of the polymers in order to figure out the applicability as solid polymer electrolyte. One of the important steps in that is to find the Glass transition temperature (T_g) and whether the polymers are in an amorphous state. Next, confirming the phase separation of the hydrophilic and hydrophobic domains is important for ionic conductivity throught the hydrophillic parts as is shown in multiple other reports. [6, 16, 27, 23] This was done by using Scanning Electron Microscopy (SEM) instead of Transmission electron microscopy (TEM) like these reports for reasons explained in section 3.2.3.

3.2.1 Thermogravimetric analysis (TGA)

Thermogravimetric analysis (TGA) was solely performed in order to find the 3% weight reduction at which point the loss in weight would be the maximum achievable temperature for a DSC-analysis. As can be seen in figure 20, the weight-loss already starts at 100 °C for some polymers. This is attributed to the presence of water and the evaporation of that water. This is influencing some results, however, as can be read in section 3.2.2, the heat-cool-heat cycle will be 110 °C at max. The 3% weight loss is found by the method found in figure 21.

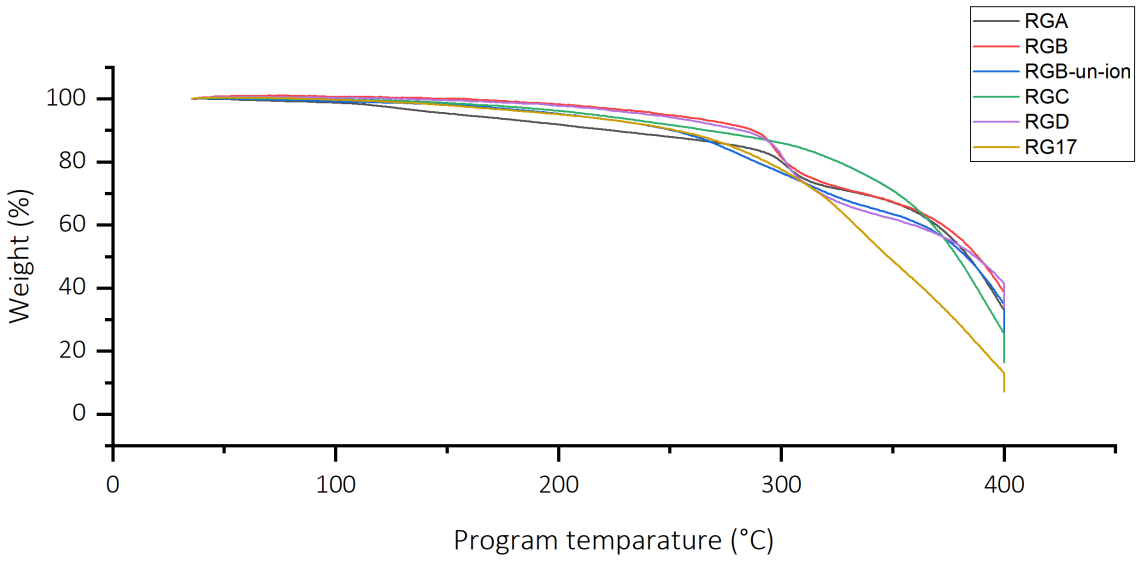

Figure 20: The results of the TGA

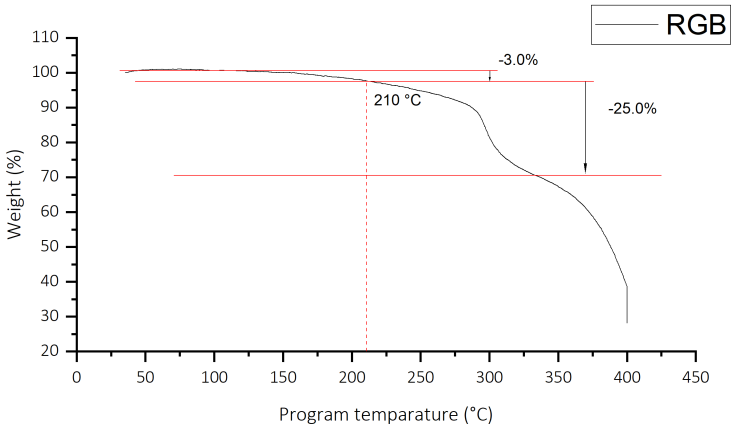

Figure 21: An example of a processed TGA result

Table 10 shows the TGA results as well as the DSC-results. It can be observed that the decomposition temperature is lower for RGA, however, this is attributed to evaporation of water. As can also been seen, the more AMPS is present, the higher the decomposition temperature. *'RGB-un-ion'* (seen in figure 20) is the RGB compound where the ion exchange was not yet performed on, to investigate whether the introduction of lithium would have influence on the T_g. The decomposition temperature of RGB-un-ion is found to be 170 °C, which is lower than the RGB compound with lithium. The reason could be that lithium is influencing the decomposition temperature since the temperature for RG17 is also around that temperature.

Table 10: Important data of the polymers.

	DSC results	TGA results	
	T_g (°C)	Decomposition temperature (°C)	Ratio [EO]:[Li^+]
RG17	-63	162	100:1
RGA	-57	132	50:1
RGB	-55	210	30:1
RGC	-62	185	84:1
RGD	-60	210	15:1

3.2.2 Differential scanning calorimetry (DSC)

After the decomposition temperatures were determined by TGA, the next step was to investigate the Glass transition temperature (T_g) of the polymers to determine whether they are in the amorphous state. The analysis cycle for the DSC was based on the investigation of Bates et al. [27] Here, the method of choice was a heat-cool-heat-cool-heat cycle with a minimum temperature of $-80\,^{\circ}C$ and a maximum temperature of $120\,^{\circ}C$. The glass transition temperatures they observe depend on the LiTFSI present within the polymer chain, but it is for all their measurements below $0\,^{\circ}C$. So, with that information, the heat-cool-heat cycle of choice would be a minimum temperature of $-90\,^{\circ}C$ and a maximum of $110\,^{\circ}C$. Also, the rate was set at $5\,^{\circ}C/min$ because a higher rate made the T_g non-observable. In figure 22, a processed DSC result can be seen where the point of inflection is found to be the glass transition temperature. The small dip before the point of inflection is observed as a 'start-up hook'. [42] All the other DSC-results can be found in appendix B.2. Bates et al. observed a T_g of $-50\,^{\circ}C$ for a polymer with [EO]:[Li^+] ratio of $-50\,^{\circ}C$ which would be the the lowest T_g they found. RGD is the closest to that [EO]:[Li^+] ratio and has a lower T_g. The reason for that might be because Bates et al. used a higher ratio of polystyrene for their polymer. As can be seen in table 10, there is no trend between [EO][Li^+] ratio and T_g. It is known that the T_g of Polyethylene oxide is around $-60\,^{\circ}C$, depending on the molecular weight of the tested polymer. So it is thought that the influence of styrene, AMPS and Li^+ is negligible in the tested ratio's. Dynamic mechanical analysis (DMA) could not be performed for analysis method, because there was not enough material to test it with.

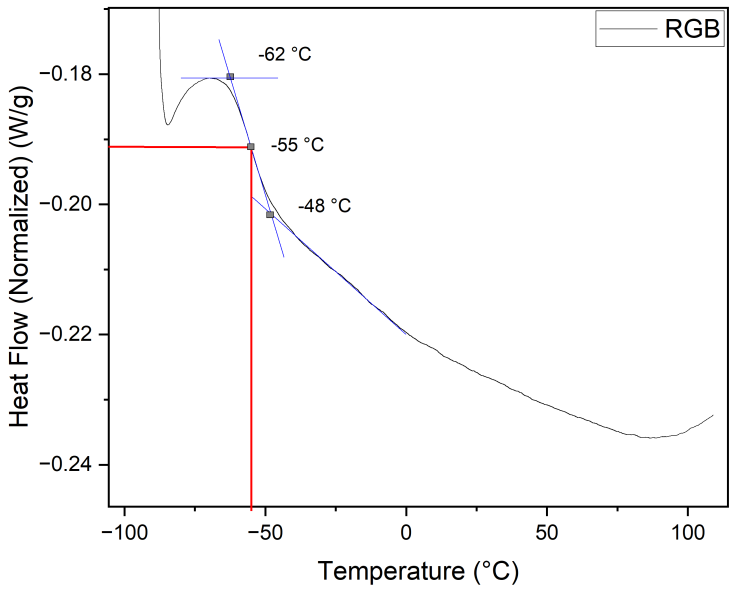

Figure 22: An example of a processed DSC result

3.2.3 Scanning Electron Microscopy (SEM)

In order to confirm the presence of nano-domains based on phase separated blocks of the prodcued block-copolymers, Scanning Electron Microscopy (SEM) was performed. Having a pure and separated hydrophilic from the hydrophobic block is necessary for unhindered and high ionic conductivity through the hydrophilic part, together with mechanical strength of the hydrophobic part. At first, TEM was tried with the help of dr. M.C.A. Stuart of the University of Groningen. It was, however, impossible to embed the polymer at room temperature and trying to find the optimum temperature for cryo-microtome was impossible to find due to time restrictions. Cryo-microtome was necessary due to the amorphous state of the polymer, making it difficult to slice a flat surface, as was experienced by Beaudoin et al. [24] So, for that reason Scanning Electron Microscopy (SEM) was seen as the most viable second option since others have used it on similar investigations, as can be seen in figure 23. SEM has as downside that it can only focus on the surface of the specimen. As explained, slicing the polymers is difficult, so examining the middle of a polymer grain was not possible. For that reason only the surface of the polymer grain could be investigated. The SEM results can be seen in figure 24a On that scan, a homogeneous surface with no visible phase separation is observed. This is based on the investigation by Niitani et al which where looking for the ratio between polystyrene and PEO and the resulting phase separation. In figure 23a a non-phase separated polymer was observed and in figure 23c, a clear phase separation was visible. According to Niitani et al., this is caused by the polystyrene content in comparison with the PEO content which should be around 50%-50%. So this, unfortunately, proofs that there is no phase-separation.

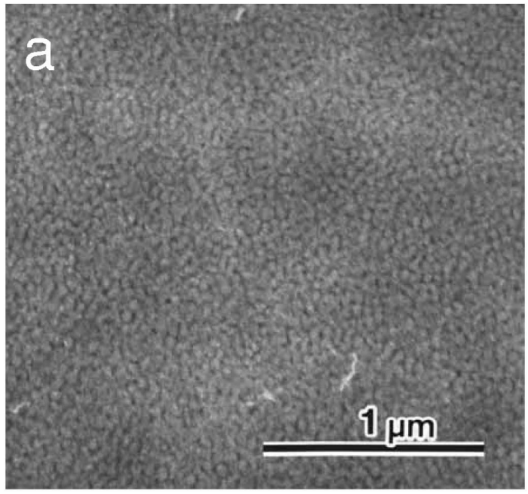

(a) A TEM image of a triblock-copolymer of PSt-b-PEGMA-b-PSt from Niitani et al. [16] where the ratio of styrene is too low. (70% PEO content)

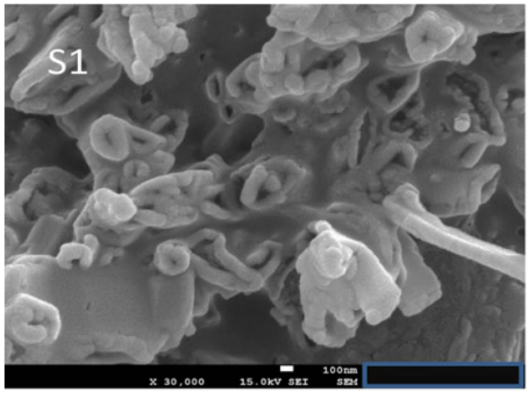

(b) SEM imagery of a block-copolymer containing PEGMA and LiAMPS from Gunday et al. [26]

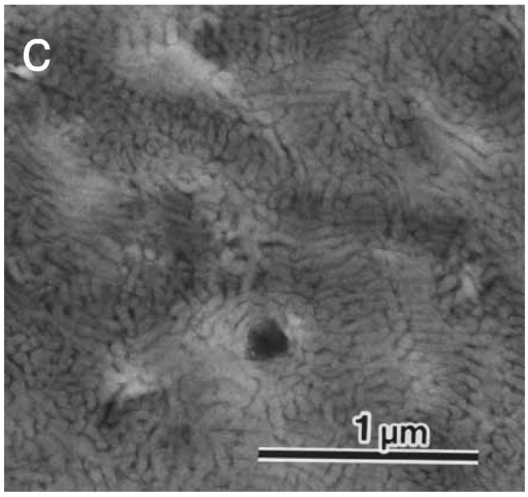

(c) TEM imagery of clear phase separated triblock-copolymer of PSt-b-PEGMA-b-PSt. Here, the amount of styrene within the polymer chain is high enough. (30-50% PEO content)

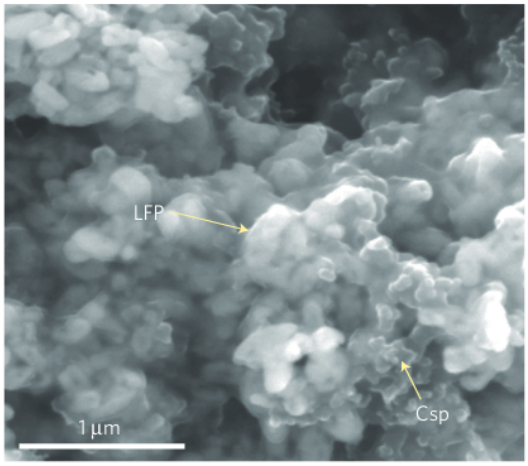

(d) SEM imagery of P(STFSILi)-b-PEO-b-P(STFSILi) triblock-copolymer obtained from Bouchet et al. [25].

Figure 23: Examples of electron microscopy pictures obtained from similar polymers investigated for SPE applications.

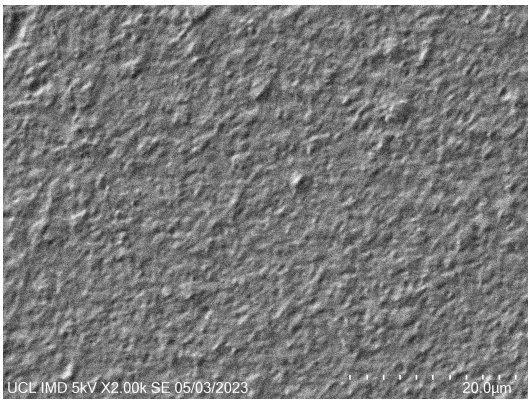

(a) RGB 2.0k magnified

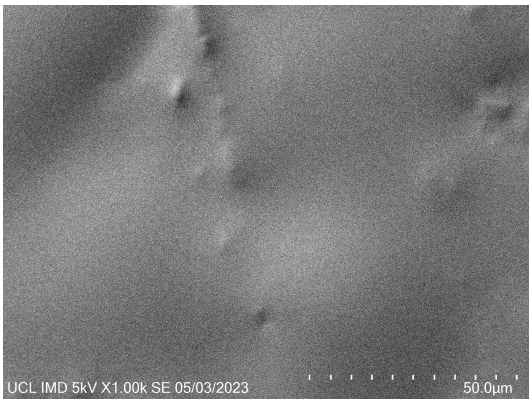

(b) RGC 1.0k magnified

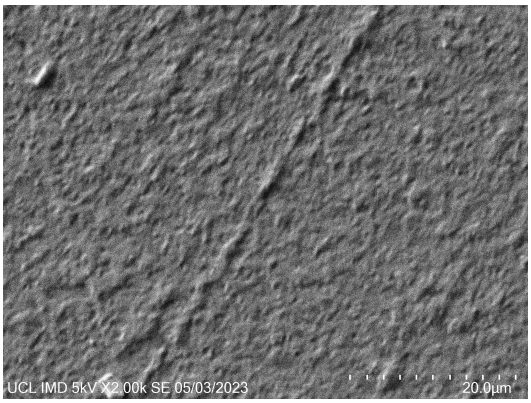

(c) RGB 2.0k magnified

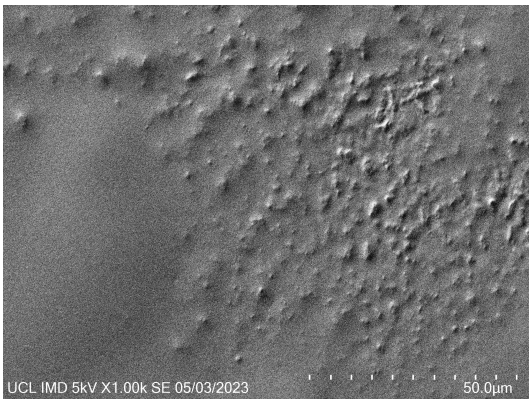

(d) RGC 1.0k magnified

Figure 24: SEM imagery obtained from UCL.

3.3 Electrochemical characterization

3.3.1 Electrochemical impedance spectroscopy (EIS)

EIS-analysis has successfully been performed on RGB and RGC by the help of dr. Georgios Nikiforidis of the University College of London. By providing the maximum achievable temperature before decomposition it was decided to perform the analysis by incriminating the temperature towards this temperature in steps and measure the effect. The cells were prepared by adding a piece of solid polymer to a Swagelok cell and the electrodes are made of stainless steel. The resulting resistances are measured according to the semi-circle method as can be seen in figure 26a where the Nyquist plot of RGB at 115 °C is analyzed. Using the plateau method on the Bode-plot was also a possibility and would give the same answer, as can be seen in figure 26b. This method was used by Bates et al. in their research. [27]

Table 11: The dimensions of the tested polymers

	RGB	RGC
Thickness [l] (cm)	1.7	1.1
Area [A] (cm^2)	0.5	1.3

The resulting impedance is processed according to the method described in section 1.7. All the results of the EIS measurements can be found in appendix C. The R_1 values of all the polymers have been used in formula 8 and these values have been plotted in the graph seen in figure 27 on page 50.

Table 12: Important results of similar investigations

	Size (kDa)	Conductivity ($S\,cm^{-1}$)	T_g (°C)	T_m (°C)
Bates [27]	300 kDa	1.00×10^{-3}	-38	
Sadoway [23]		9.00×10^{-4}	-60	
Beaudoin [24]	35 kDa	-		64
Bouchet 2013 [25]		1.30×10^{-5}		65
Bouchet 2014 [29]	35 kDa	1.00×10^{-4}		40
Gunday [26]	-	3.22×10^{-6}	-	-

The highest conductivity was found to be at 115 °C. The corresponding Nyquist plots are found in figure 25. In this plot it can already be seen that the conuctivity of RGB is better than the conductivity for RGC. This alligns with the conductivity's found by other sources [27, 23, 24] where the ideal ratio between [EO]:[Li^+] is found to be around 20:1. RGB has a ratio of 30:1, which is less favourable for the ionic conductivity in theory however, the rigid nature of the polymer made it difficult to prepare it in the Swagelok cell. This is the reason why there is no data on this polymer. Therefor, in this research it is found that RGB with the aforementioned [EO]:[Li^+] ratio is the polymer with the highest conductivity tested.

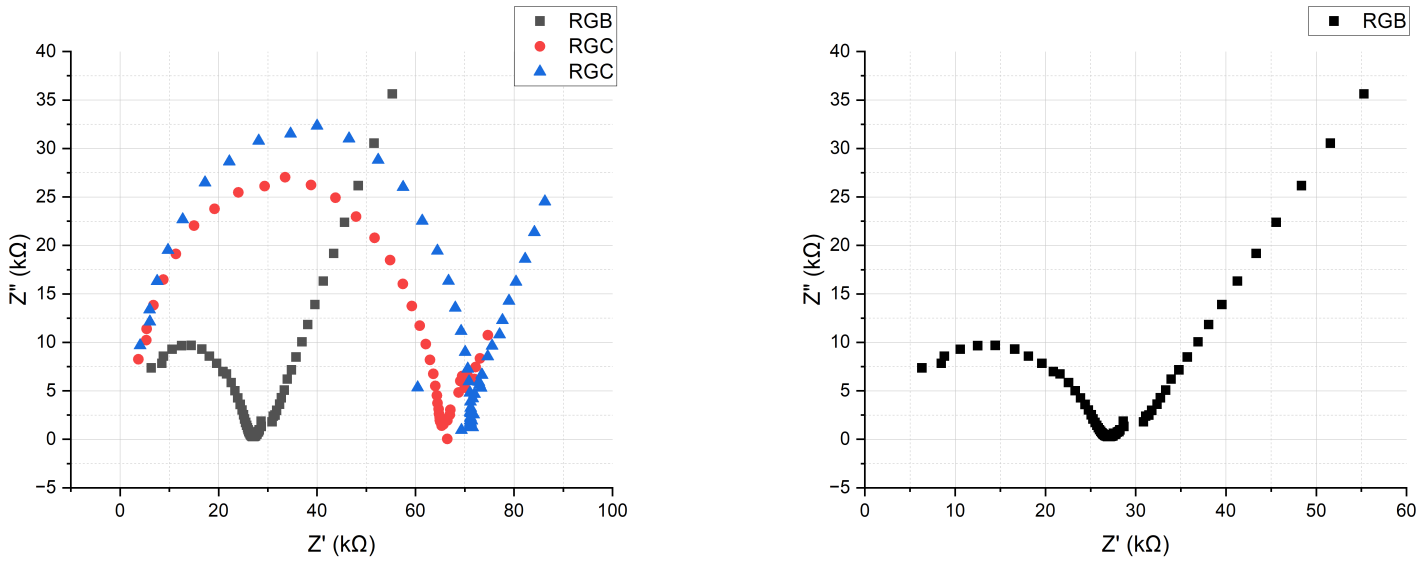

Figure 25: The EIS results at 115 °C. The EIS results for lower temperatures can be found in appendix C

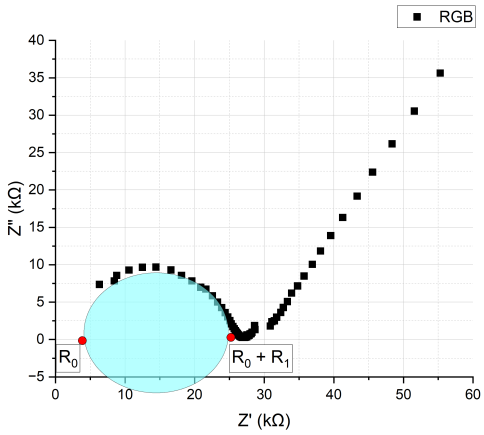

(a) The resulting Nyquist plot obtained from the EIS measurement is analyzed with the semi-circle method similar to how Huggins et al. proposed the method. [43] R_0 is the inherent resistance from the electrode of the used apparatus. R_1 is the resistance of interest. Note that the Nyquist plot is not reaching a perfect semi-circle, hence the addition of a circle to make both points of interest more clear.

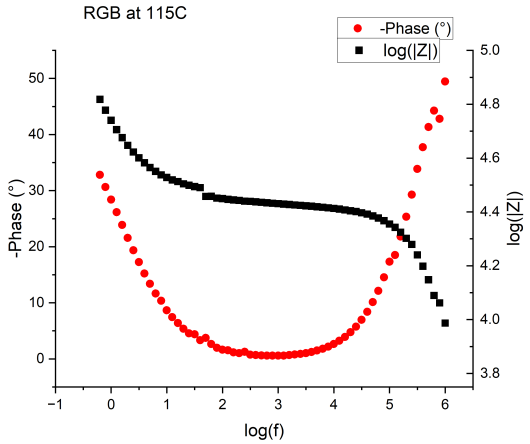

(b) The Bode plot of RGB at 115 °C where the high frequency plateau of the Bode plot is the same impedance value of the Nyquist plot.

Figure 26: Results of the EIS

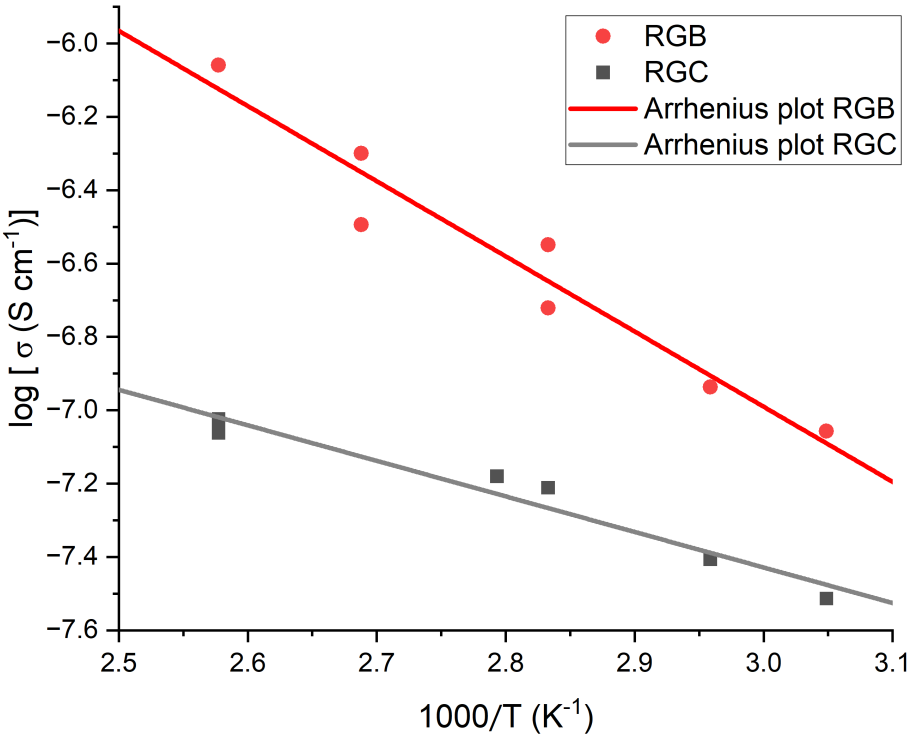

Figure 27: The Arrhenius fit on the EIS-spectra of the two tested polymers. The corresponding EIS-spectra can be found in appendix C.

RGB

Arrhenius fit $\sigma_{ion}(T) = \sigma_0 - (\frac{0.4343 \times E_A \times x}{8.314})$
E_A = 39.237 kJ/mole
σ_0 = -0.841 (S/cm)

RGC

Arrhenius fit $\sigma_{ion}(T) = \sigma_0 - (\frac{0.4343 \times E_A \times x}{8.314})$
E_A = 18.552 kJ/mole
σ_0 = -4.521 (S/cm)

Cycleability test

There was no opportunity to test the cycleability unfortunately, however, there is much to improve on the polymer design before there is relevance into testing the cycleability.

3.4 Discussion

The important reason why the polymer was designed as it is was to create nano-domains, or in other words, to produce a supramolecular structure where hydrophobic parts would provide the mechanical strength for the ionic conductivity in the hydrophilic part. Through SEM data it became clear that this was unfortunately not achieved. Furthermore, there was no T_g visible of styrene, meaning the influence of styrene was too low as well. The reason could be that the DP of the styrene blocks was too small like is discussed by Niitani et al.[16, 44] This could also explain the poor solubility of the polymers within all the available solvent, since both the hydrophobic and hydrophilic domains would hinder interaction with a solvent between one another. The DP of the whole polymer was long considered to be the cause of this issue, however, as is visible in table 12 multiple reports used polymers of larger sizes with more promising results. There is therefore a causal relationship between the failed phase separation and the ratio between the hydrophobic and hydrophilic blocks. Next, the ability to dissociate between the ionic parts is also investigated to be of great importance [45, 46, 47]. This is the ability of the anionic part to displace its charge over the molecule and to retain its stability. $^{-}$TFSI is one of the most advanced lithium salt anions for its high ion dissociation constant and donor number. The reports with high lithium-ion conductivity mainly used this ionic liquid. Furthermore, bistriflimide is also acting as plasticizer. [46, 47] The plasticizer incorporated within the hydrophilic part that tend to crystallize, is a great tool to prevent that crystallization kinetics to occur. This ability translates into great ionic conductivity. The slow titration of the lithium hydroxide with the protonated triethylamine could have been caused by the poor dissociation kinetics.

Aprotic protic

The used polymer and its process to produce it is very proton rich. This could be a problem for long term usage since the protons can interact with the metal electrodes. Aprotic ionic liquids have been tested before and resulted in

4 Recommendations

As mentioned in the discussion, the phase separation was not visible on the SEM. It is thought that this means that the phase separation failed. A reason to overcome this in the future is to introduce longer hydrophobic parts within the polymer. This is experimentally confirmed to benefit the phase separation. Next to the introduction of a longer hydrophobic part, it is also necessary to introduce a form of plasticizer to the hydrophilic part in order to hinder to crystallinity in the hydrophilic phase in the PEO part. This can easily be achieved by introducing it in the chain propagation. Solubility is predicted to be enhanced when introducing these plasticizers as well. However, when this is not the case, the size of the polymer could be on a too large size which could cause too much intermolecular interactions. The titration of the lithium hydroxide happened in an aqueous environment. It is interesting to investigate the influence of titrating it in an organic phase with lithium-hydride. Introducing the lithium-hydride to the protonated triethylamine would lead to producing hydrogen and gaseous triethylamine. This would prevent water to be introduced to the electrolyte and would probably benefit the ion conductivity. When solubility is still poor, it is also recommended to perform the GPC analysis on the polymers that are still within the reaction mixture. At this point the polymer is generally completely dissolved, so this would make the complete dissolution more probable. The polymers that were produced had a rigid feel to it. The actual physical modulus was not tested due to it there was not enough product to test it with. Therefor, it might be interesting to test the products on a Dynamic Mechanical Analysis (DMA) set-up. This is a method to find the Tg and also the modulus, two very important characteristics of a SPE. Another interesting characterization is cyclic voltammetry where the maximum voltage on the system is tested.

5 Conclusion

Block co-polymers are an increasingly more interesting way to produce sturdy solid polymer electrolyte (SPE) membranes for lithium-ion battery application. Although research is limited, the promise of higher conductivity with this method is evident. A supra-molecular structure formed by the hydrophilic/hydrophobic interactions of the polymer blocks, gives interesting behaviour where the soft hydrophilic part facilitates the ionic conductivity and the hydrophobic part the mechanical strength to prevent dendritic growth of lithium between the electrodes. In this research, PSt-*b*-PEGMA-*r*-AMPS-*b*-PSt was produced using the RAFT-polymerization technique. The AMPS-monomer was polymerized with protonated Et_3N being the counter-ion and subsequently exchanged for Li^+ in a base titration where Et_3N left the mixture as an immiscible gas. DMAcTTC was used as the RAFT-agent, which made it possible to propagate the chain from the middle and with that equal lengths of the Polystyrene parts of the polymer. Due to poor solubillity of the polymers, it became impossible to determine the molecular weights based on GPC, however, it was possible to do GPC on the macroCTA. The molecular weights of the polymers was estimated based on the added molar amounts and the conversion of the monomers, which was determined using ^{1}H-NMR. DOSY was used to determine the dispersion of molecular weight and potentially find the PDI. ICP-MS was used to determine the success of the neutralization of the AMPS which was found to be in accordance with the prediction. In order to find the decomposition temperatures and the Glass transition temperature (T_g), Thermogravimetric analysis (TGA) and Differential scanning calorimetry (DSC) were used respectively. The decomposition temperatures were on average around 150 °C and the T_g's were all around −60 °C which is similar to other reports. These data was important for the Electrochemical impedance spectroscopy (EIS) to investigate the ionic conductivity of the polymers containing AMPS. This was only done of RGB and RGC due to limitations on the measurements. It was found that RGB → PSt_{27}-*b*-$PEGMA_{156}$-*r*-$AMPS_{54}$-*b*-PSt_{27} with [EO]:[Li] to be 30:1 at 115 °C gave the highest ionic conductivity of $8.720 \times 10^{-7}\,\mathrm{S\,cm^{-1}}$.

6 Acknowledgements

During my thesis I had the privilege of working on a topic that was completely designed by myself with the help, the supervision and most importantly the approval and support by prof. dr. Patrizio Raffa and his colleague dr. Vassilis Kyriakou. There were many unknown obstacles and issues that had to be dealt with during my 8 months of research. Both prof. Raffa and dr. Kyriakou were flexible and supportive during this period and provided me with solutions that would benefit the resulting report. In this time, I also had the privilege to work with Alex Guzik who had guided me through the process of RAFT polymerization, the characterization of the resulting polymers and the general guidance for the synthesis. In the process of characterization, I had to gain knowledge into new analysis techniques which gave me not only results for my thesis, but would also be of great importance for my future career. For that, I would like to thank Gert-Jan Boer and Leon Rohrbach who were not only great persons to work with but also very insightful and helpful. In the process of analyzing my produced polymers I also learned new techniques for NMR. The input and the effort made by ing. Pieter van der Meulen and dr. Johan Kemmink were second to none. My thesis revolved around the application of polymers in solid state batteries. Although the University of Groningen would give me support in nearly all aspects of this question, there were still answers to be found. A glove-box was not available which made the synthesis and testing in inert environment impossible. Dr. Vassilis Kyriakou was able to link me up with dr. Georgios Nikiforidis who not only made some analyses, he was also open to adjust the measurements to the recommendations I gave and also gave some options to me as well. I had enjoyed the last 8 months with the company I got from Fabrice, Floris and Matina. The punctual 12 PM lunch-break with the not so punctual ending will stick with me. Their help into providing me with some insights is also still visible within my report. Last but not least, I want to thank Lisanne who gave me mental support and sticked by my side during last months. She was the one who actually made these periods fun and also inspired me to make difficult steps in some points.

References

[1] The Nobel Prize, "The Nobel Prize in Chemistry 2019," Oct. 2019.

[2] UN, Department of Economic and Social Affairs, Hiroshi Kawamura, Marcelo LaFleur, Kenneth Iversen, and Hoi Wai Jackie Cheng, "Frontier Technology Issues: Lithium-ion batteries: a pillar for a fossil fuel-free economy?," July 2021.

[3] Jakob Fleischmann, Mikael Hanicke, Evan Horetsky, Dina Ibrahim, Sören Jautelat, Martin Linder, Patrick Schaufuss, Lukas Torscht, and Alexandre van de Rijt, "Lithium-ion battery demand forecast for 2030 | McKinsey."

[4] M. A. Hannan, M. M. Hoque, A. Hussain, Y. Yusof, and P. J. Ker, "State-of-the-Art and Energy Management System of Lithium-Ion Batteries in Electric Vehicle Applications: Issues and Recommendations," *IEEE Access*, vol. 6, pp. 19362–19378, 2018.

[5] B. Simon, S. Flandrois, K. Guerin, A. Fevrier-Bouvier, I. Teulat, and P. Biensan, "On the choice of graphite for lithium ion batteries," *Journal of Power Sources*, vol. 81-82, pp. 312–316, Sept. 1999.

[6] P. Raghavan and J. F. M. J, eds., *Polymer electrolytes for energy storage devices.* Boca Raton: CRC Press, first edition ed., 2021.

[7] CPSC, "CPSC Calls on Manufacturers to Comply with Safety Standards for Battery-Powered Products to Reduce the Risk of Injury and Death," Dec. 2022.

[8] C. Heubner, M. Schneider, and A. Michaelis, "Diffusion-Limited C-Rate: A Fundamental Principle Quantifying the Intrinsic Limits of Li-Ion Batteries," *Advanced Energy Materials*, vol. 10, p. 1902523, Jan. 2020.

[9] D. Cao, X. Sun, Q. Li, A. Natan, P. Xiang, and H. Zhu, "Lithium Dendrite in All-Solid-State Batteries: Growth Mechanisms, Suppression Strategies, and Characterizations," *Matter*, vol. 3, pp. 57–94, July 2020.

[10] R. Xiong, S. Ma, H. Li, F. Sun, and J. Li, "Toward a Safer Battery Management System: A Critical Review on Diagnosis and Prognosis of Battery Short Circuit," *iScience*, vol. 23, p. 101010, Apr. 2020.

[11] C. Li, Z.-y. Wang, Z.-j. He, Y.-j. Li, J. Mao, K.-h. Dai, C. Yan, and J.-c. Zheng, "An advance review of solid-state battery: Challenges, progress and prospects," *Sustainable Materials and Technologies*, vol. 29, p. e00297, Sept. 2021.

[12] Frank E. Swindells, J. A. Maloney, and Gerald Halspert, "INVESTIGATION OF SOLID STATE ELECTROLYTE SILVER-ZINC BATTERY," tech. rep., MELPAR (NASA), Falls Church, VI, USA, Mar. 1970.

[13] Z. Xue, D. He, and X. Xie, "Poly(ethylene oxide)-based electrolytes for lithium-ion batteries," *Journal of Materials Chemistry A*, vol. 3, no. 38, pp. 19218–19253, 2015.

[14] B. A. Maia, N. Magalhães, E. Cunha, M. H. Braga, R. M. Santos, and N. Correia, "Designing Versatile Polymers for Lithium-Ion Battery Applications: A Review," *Polymers*, vol. 14, p. 403, Jan. 2022.

[15] Q. Guo, ed., *Polymer morphology: principles, characterization, and processing*. Hoboken, New Jersey: John Wiley & Sons, 2016.

[16] T. Niitani, M. Shimada, K. Kawamura, and K. Kanamura, "Characteristics of new-type solid polymer electrolyte controlling nano-structure," *Journal of Power Sources*, vol. 146, pp. 386–390, Aug. 2005.

[17] A.-V. G. Ruzette, P. P. Soo, D. R. Sadoway, and A. M. Mayes, "Melt-Formable Block Copolymer Electrolytes for Lithium Rechargeable Batteries," *Journal of The Electrochemical Society*, vol. 148, no. 6, p. A537, 2001.

[18] S. Perrier, "*50th Anniversary Perspective* : RAFT Polymerization—A User Guide," *Macromolecules*, vol. 50, pp. 7433–7447, Oct. 2017.

[19] B. D. Fairbanks, P. A. Gunatillake, and L. Meagher, "Biomedical applications of polymers derived by reversible addition – fragmentation chain-transfer (RAFT)," *Advanced Drug Delivery Reviews*, vol. 91, pp. 141–152, Aug. 2015.

[20] S. P. Moulik, A. K. Rakshit, A. Pan, and B. Naskar, "An Overview of Coacervates: The Special Disperse State of Amphiphilic and Polymeric Materials in Solution," *Colloids and Interfaces*, vol. 6, p. 45, Sept. 2022.

[21] L. Voorhaar and R. Hoogenboom, "Supramolecular polymer networks: hydrogels and bulk materials," *Chemical Society Reviews*, vol. 45, no. 14, pp. 4013–4031, 2016.

[22] M. Hetzer, B. V. K. J. Schmidt, C. Barner-Kowollik, and H. Ritter, "Supramolecular polymer networks of building blocks prepared via RAFT polymerization," *Polymer Chemistry*, vol. 5, no. 6, p. 2142, 2014.

[23] D. R. Sadoway, "Block and graft copolymer electrolytes for high-performance, solid-state, lithium batteries," *Journal of Power Sources*, vol. 129, pp. 1–3, Apr. 2004.

[24] E. Beaudoin, T. N. T. Phan, M. Robinet, R. Denoyel, P. Davidson, D. Bertin, and R. Bouchet, "Effect of Interfaces on the Melting of PEO Confined in Triblock PS- *b* -PEO- *b* -PS Copolymers," *Langmuir*, vol. 29, pp. 10874–10880, Aug. 2013.

[25] R. Bouchet, S. Maria, R. Meziane, A. Aboulaich, L. Lienafa, J.-P. Bonnet, T. N. T. Phan, D. Bertin, D. Gigmes, D. Devaux, R. Denoyel, and M. Armand, "Single-ion BAB triblock copolymers as highly efficient electrolytes for lithium-metal batteries," *Nature Materials*, vol. 12, pp. 452–457, May 2013.

[26] S. T. Gunday, A. Z. Kamal, M. A. Almessiere, S. Çelik, and A. Bozkurt, "An investigation of lithium ion conductivity of copolymers based on P(AMPS-co-PEGMA)," *Journal of Applied Polymer Science*, vol. 136, p. 47798, Aug. 2019.

[27] C. M. Bates, A. B. Chang, N. Momčilović, S. C. Jones, and R. H. Grubbs, "ABA Triblock Brush Polymers: Synthesis, Self-Assembly, Conductivity, and Rheological Properties," *Macromolecules*, vol. 48, pp. 4967–4973, July 2015.

[28] X.-B. Cheng, C.-Z. Zhao, Y.-X. Yao, H. Liu, and Q. Zhang, "Recent Advances in Energy Chemistry between Solid-State Electrolyte and Safe Lithium-Metal Anodes," *Chem*, vol. 5, pp. 74–96, Jan. 2019.

[29] R. Bouchet, T. N. T. Phan, E. Beaudoin, D. Devaux, P. Davidson, D. Bertin, and R. Denoyel, "Charge Transport in Nanostructured PS–PEO–PS Triblock Copolymer Electrolytes," *Macromolecules*, vol. 47, pp. 2659–2665, Apr. 2014.

[30] P. Vadhva, J. Hu, M. J. Johnson, R. Stocker, M. Braglia, D. J. L. Brett, and A. J. E. Rettie, "Electrochemical Impedance Spectroscopy for All-Solid-State Batteries: Theory, Methods and Future Outlook," *ChemElectroChem*, vol. 8, pp. 1930–1947, June 2021.

[31] M. E. Orazem and B. Tribollet, *Electrochemical impedance spectroscopy*. Hoboken, New Jersey: John Wiley & Sons, Inc, 2nd edition ed., 2017.

[32] Q.-C. Zhuang, X.-Y. Qiu, S.-D. Xu, Y.-H. Qiang, and S.-G. Su, "Diagnosis of Electrochemical Impedance Spectroscopy in Lithium-Ion Batteries," in *Lithium Ion Batteries - New Developments* (I. Belharouak, ed.), InTech, Feb. 2012.

[33] N. Kamaya, K. Homma, Y. Yamakawa, M. Hirayama, R. Kanno, M. Yonemura, T. Kamiyama, Y. Kato, S. Hama, K. Kawamoto, and A. Mitsui, "A lithium superionic conductor," *Nature Materials*, vol. 10, pp. 682–686, Sept. 2011.

[34] J. Liang, G.-r. Shan, and P.-j. Pan, "Aqueous RAFT polymerization of acrylamide: A convenient method for polyacrylamide with narrow molecular weight distribution," *Chinese Journal of Polymer Science*, vol. 35, pp. 123–129, Jan. 2017.

[35] A. Guzik and P. Raffa, "Direct synthesis *via* RAFT of amphiphilic diblock polyelectrolytes facilitated by the use of a polymerizable ionic liquid as a monomer," *Polymer Chemistry*, vol. 12, no. 38, pp. 5505–5517, 2021.

[36] D. J. Peterson and N. M. Loening, "QQ-HSQC: a quick, quantitative heteronuclear correlation experiment for NMR spectroscopy," *Magnetic Resonance in Chemistry*, vol. 45, pp. 937–941, Nov. 2007.

[37] K. Hu, J. J. Ellinger, R. A. Chylla, and J. L. Markley, "Measurement of Absolute Concentrations of Individual Compounds in Metabolite Mixtures by Gradient-Selective Time-Zero ^{1} H– ^{13} C HSQC with Two Concentration References and Fast Maximum Likelihood Reconstruction Analysis," *Analytical Chemistry*, vol. 83, pp. 9352–9360, Dec. 2011.

[38] K. Hu, W. M. Westler, and J. L. Markley, "Simultaneous Quantification and Identification of Individual Chemicals in Metabolite Mixtures by Two-Dimensional Extrapolated Time-Zero ^{1} H ^{13} C HSQC (HSQC $_{0}$)," *Journal of the American Chemical Society*, vol. 133, pp. 1662–1665, Feb. 2011.

[39] Y. Zhou, Z. Wang, J. Wu, J. Wang, and H. Zhao, "Saturated Solubility of 2-Acrylamide-2-methylpropanesulfonic Acid in 14 Neat Organic Solvents from 283.15 to 328.15 K," *Journal of Chemical & Engineering Data*, vol. 65, pp. 4692–4698, Sept. 2020.

[40] PubChem, "Triethylamine."

[41] J. Viéville, M. Tanty, and M.-A. Delsuc, "Polydispersity index of polymers revealed by DOSY NMR," *Journal of Magnetic Resonance*, vol. 212, pp. 169–173, Sept. 2011.

[42] TA Instruments, "Interpreting Unexpected Events and Transitions in DSC Results."

[43] R. A. Huggins, "Simple method to determine electronic and ionic components of the conductivity in mixed conductors a review," *Ionics*, vol. 8, pp. 300–313, May 2002.

[44] T. Niitani, M. Shimada, K. Kawamura, K. Dokko, Y.-H. Rho, and K. Kanamura, "Synthesis of Li+ Ion Conductive PEO-PSt Block Copolymer Electrolyte with Microphase Separation Structure,"

[45] A. Arya and A. L. Sharma, "A glimpse on all-solid-state Li-ion battery (ASSLIB) performance based on novel solid polymer electrolytes: a topical review," *Journal of Materials Science*, vol. 55, pp. 6242–6304, May 2020.

[46] S. Lascaud, M. Perrier, A. Vallee, S. Besner, J. Prud'homme, and M. Armand, "Phase Diagrams and Conductivity Behavior of Poly(ethylene oxide)-Molten Salt Rubbery Electrolytes," *Macromolecules*, vol. 27, pp. 7469–7477, Dec. 1994.

[47] A. Vallée, S. Besner, and J. Prud'Homme, "Comparative study of poly(ethylene oxide) electrolytes made with LiN(CF3SO2)2, LiCF3SO3 and LiClO4: Thermal properties and conductivity behaviour," *Electrochimica Acta*, vol. 37, pp. 1579–1583, Jan. 1992.

A Appendix I

A.1 Target components

Table 13: The targeted amounts of components needed for the initial reaction as described in chapter 2

		mL added	(g) added	mole
RG17	AMPS	0,000	0,000	0,000E+00
	PEGMA	4,725	5,198	1,040E-02
	ACVA	2,80E-03	2,80E-03	9,990E-06
	DIOX	3,049	3,140	3,564E-02
	MacroCTA	0,403	0,403	6,953E-05
RGA	AMPS	0,563	0,619	2,987E-03
	PEGMA	5,929	6,522	1,304E-02
	ACVA	4,03E-03	4,03E-03	1,438E-05
	DIOX	3,05	3,142	3,565E-02
	MacroCTA	4,02E-01	0,40228	6,936E-05
	Et3N	0,47	0,341	3,372E-03
RGB	AMPS	0,564	0,991	4,782E-03
	PEGMA	5,534	6,087	1,217E-02
	ACVA	4,30E-03	4,30E-03	1,534E-05
	DIOX	3,05	3,142	3,565E-02
	MacroCTA	4,29E-01	0,42909	7,398E-05
	Et3N	0,667	0,484	4,785E-03
RGC	AMPS	0,564	0,291	1,404E-03
	PEGMA	6,278	6,906	1,381E-02
	ACVA	3,79E-03	3,79E-03	1,352E-05
	DIOX	3,052	3,144	3,568E-02
	MacroCTA	3,79E-01	3,79E-01	6,528E-05
	Et3N	0,196	0,142	1,406E-03
RGD	AMPS	0,564	1,905	9,192E-03
	PEGMA	4,561	5,017	1,003E-02
	ACVA	4,96E-03	4,96E-03	1,770E-05
	DIOX	3,039	3,130	3,553E-02
	MacroCTA	4,95E-01	4,95E-01	8,536E-05
	Et3N	1,3	0,944	9,327E-03

A.2 GPC-data

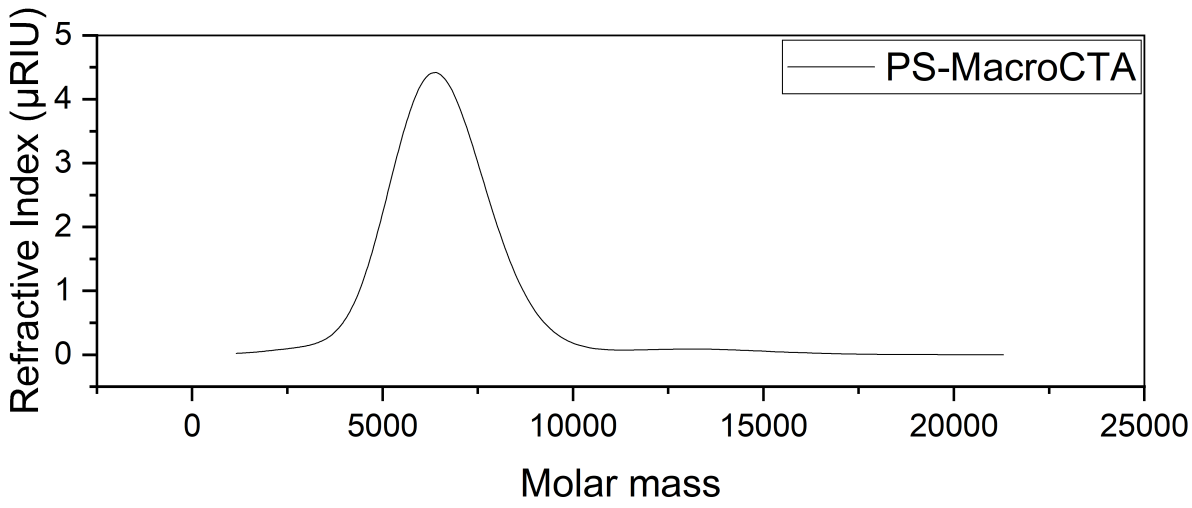

Figure 28: The results of the GPC

A.3 Styrene conversion with the MacroCTA

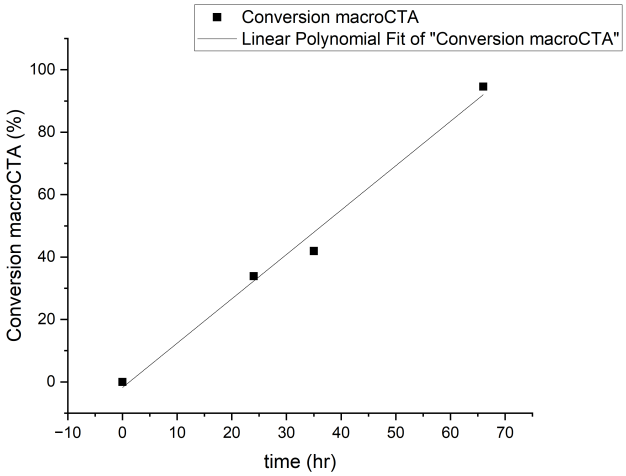

Styrene

Conversion fit $y = -1.82 + 1.42x$

$t_{\frac{1}{2}} = 2190$ min

$k = 3.17\text{E-}4$ min^{-1}

Figure 29: Conversion of styrene with the macroCTA

Table 14: Added amounts of components and the measured conversion of the components. This was then converted to the molar weight of the polymers according to formula 10

Polymer	Compound	mL	(g) added	Mole added	Conversion (%)	mole*converted	[amps]/[pegma]	Ratio (%)	Mn,th (g/mo)
RG17	AMPS		0	0.000E+00		0.000E+00	-	0.00	158456
	PEGMA	4.7	4.7376	9.475E-03	1	9.475E-03		100.00	
	ACVA	2.80E-03	2.80E-03	9.990E-06					
	DIOX	2	2.06	2.338E-02					
	MacroCTA	0.18	0.18	3.103E-05					
RGA	AMPS	0.564	0.620	2.993E-03	93.840	2.809E-03	0.239	19.28	98733.707
	PEGMA	5.930	5.977	1.195E-02	98.370	1.176E-02		80.72	
	ACVA	4.60E-03	4.60E-03	1.641E-05					
	DIOX	3.049	3.140	3.564E-02					
	MacroCTA	0.403	0.403	6.953E-05					
RGB	AMPS	0.903	0.993	4.791E-03	83.280	3.990E-03	0.377	27.37	88438.9648
	PEGMA	5.535	5.579	1.116E-02	94.890	1.059E-02		72.63	
	ACVA	4.90E-03	4.90E-03	1.748E-05					
	DIOX	3.050	3.142	3.565E-02					
	MacroCTA	0.430	0.430	7.407E-05					
RGC	AMPS	0.267	0.293	1.416E-03	63.390	8.974E-04	0.082	7.58	92141.4842
	PEGMA	6.300	6.350	1.270E-02	86.150	1.094E-02		92.42	
	ACVA	4.00E-03	4.00E-03	1.427E-05					
	DIOX	3.100	3.193	3.624E-02					
	MacroCTA	0.380	0.380	6.552E-05					
RGD	AMPS	1.733	1.907	9.200E-03	88.980	8.186E-03	0.907	47.56	78388.936
	PEGMA	4.560	4.596	9.193E-03	98.170	9.025E-03		52.44	
	ACVA	6.90E-03	6.90E-03	2.462E-05					
	DIOX	3.300	3.399	3.858E-02					
	MacroCTA	0.496	0.496	8.553E-05					

A.4 Monomer conversion during chain extension

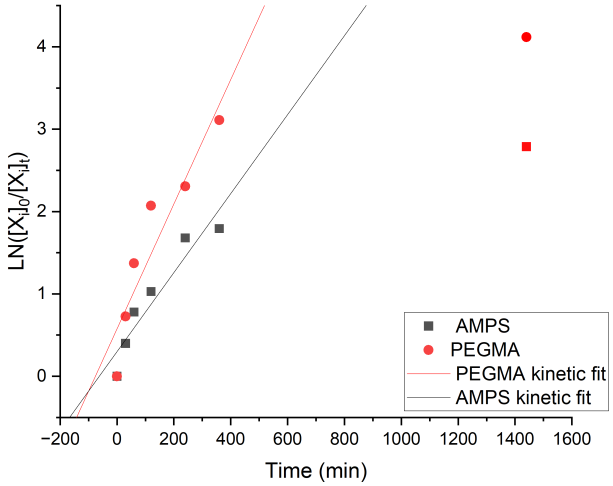

Figure 30: The found k-values are used in the formula LN($[x_i]0/[x_i]t$) for both monomers and compared with the $[x_i]$ values measured by ^{1}H-NMR. The resulting $\boldsymbol{k}$-value for PEGMA= $7.56 \times 10^{-3}\,\mathrm{min}^{-1}$, AMPS = $4.79 \times 10^{-3}\,\mathrm{min}^{-1}$. The last two datapoints were placed as outliers for the kinetic plot since end-conversion was reached before that.

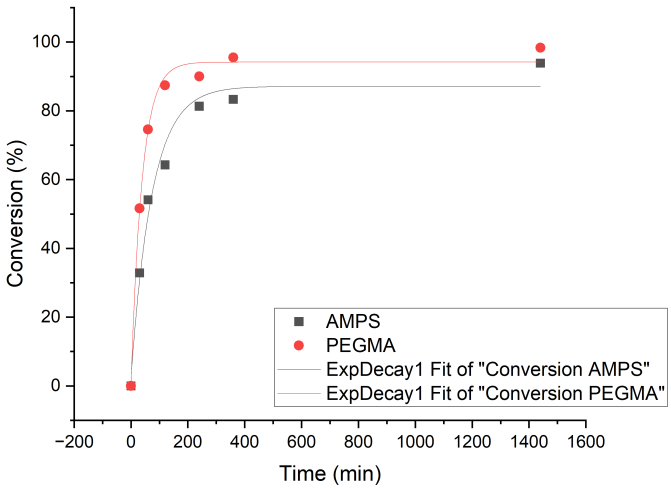

Figure 31: The conversion of both monomers over time for RGA. Conversion fit AMPS $y = 87.09 - 91.48 * exp(-\frac{x+5.7}{74.24})$ Conversion fit PEGMA $y = 94.16 - 105.79 * exp(-\frac{x+4.6}{38.77})$

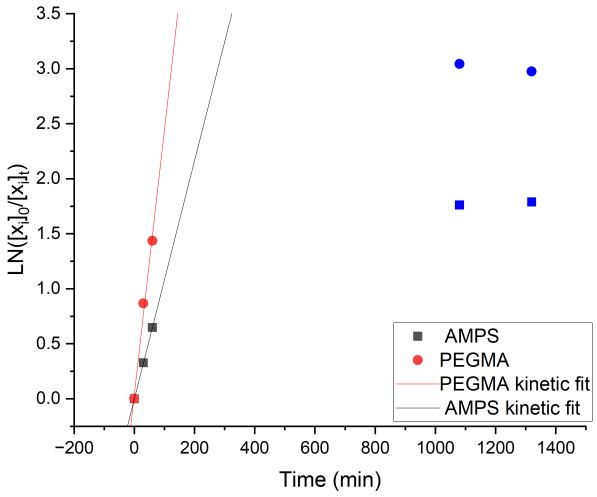

Figure 32: The found k-values are used in the formula LN($[x_i]0/[x_i]t$) for both monomers and compared with the $[x_i]$ values measured by ^{1}H-NMR. The resulting $\boldsymbol{k}$-value for PEGMA$= 2.39 \times 10^{-2}\,\mathrm{min}^{-1}$, AMPS $= 1.08 \times 10^{-3}\,\mathrm{min}^{-1}$ (However, there are not many measurement-points) The last two datapoints were placed as outliers for the kinetic plot since end-conversion was reached before that.

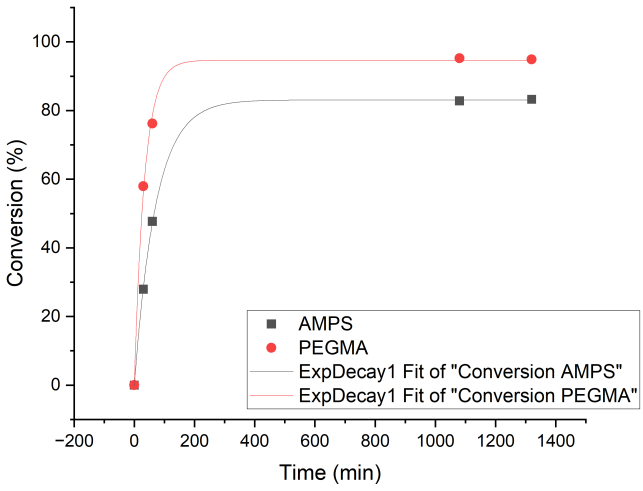

Figure 33: The conversion of both monomers over time for RGB. Conversion fit AMPS $y = 94.63 - 106.61 * exp(-\frac{x+4.2}{33.75})$ Conversion fit PEGMA $y = 83.08 - 84.78 * exp(-\frac{x+1.3}{71.08})$

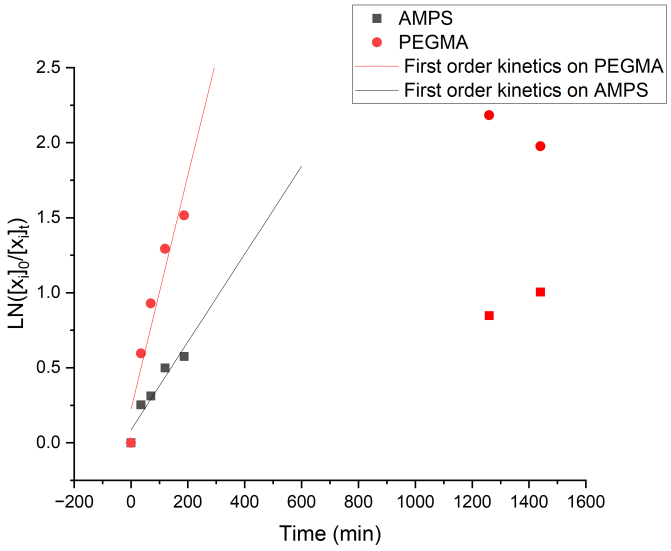

Figure 34: The found k-values are used in the formula LN($[x_i]0/[x_i]t$) for both monomers and compared with the $[x_i]$ values measured by ^{1}H-NMR. The resulting $\boldsymbol{k}$-value = PEGMA= $7.77 \times 10^{-3}\,\mathrm{min}^{-1}$, AMPS = $2.93 \times 10^{-3}\,\mathrm{min}^{-1}$ The last two datapoints were placed as outliers for the kinetic plot since end-conversion was reached before that.

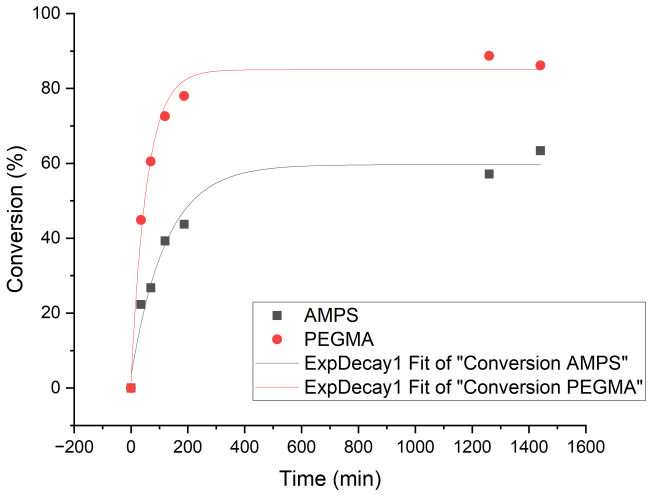

Figure 35: The conversion of both monomers over time for RGC. Conversion fit AMPS $y = 59.62 - 62.47 * exp(-\frac{x+12.1}{122.54})$ Conversion fit PEGMA $y = 84.98 - 88.28 * exp(-\frac{x+3.2}{55.64})$

For RGD there were not enough data points to find the conversionplot. In order to find a linear relationship for finding the kinetic constant, more datapoints were needed hence there is no kinetic constant found. It can be assumed though that the kinetic constant of AMPS is close to 60 min^{-1} since the data of RGA and RGB are polymers with more AMPS containing.

A.5 Extra data on CHNS-analysis

Table 15: The predicted CHNS-analysis result when twice the amount of PEGMA is present.

Element	C	H	N	S	O
Total number elements based on DP	9496	17876	86	40	4230
RAFT agent	8	14	0	3	4
Total	9504	17890	86	43	4234
Elemental weight (g/mol)	12	1	14	32	16
Total contributing weight of element (g/mol)	114048.24	17890.32	1204.63	1389.33	67750.25
wt% of element	56.38	8.84	0.60	0.69	33.49

Table 16: The predicted CHNS-analysis result when half of the AMPS is converted.

Element	C	H	N	S	O
Total number elements based on DP	4964	9154	43	20	2115
RAFT agent	8	14	0	3	4
Total	4972	9168	43	23	2119
Elemental weight (g/mol)	12	1	14	32	16
Total contributing weight of element (g/mol)	59664.12	9168.16	602.32	742.67	33907.13
wt% of element	57.32	8.81	0.58	0.71	32.58

A.6 Mechanism

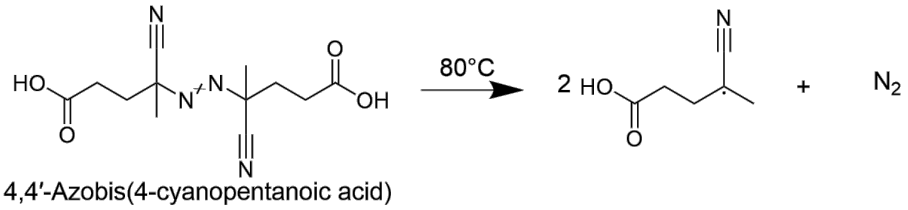

Figure 36: The initiation step where the initiator is split up in radicals.

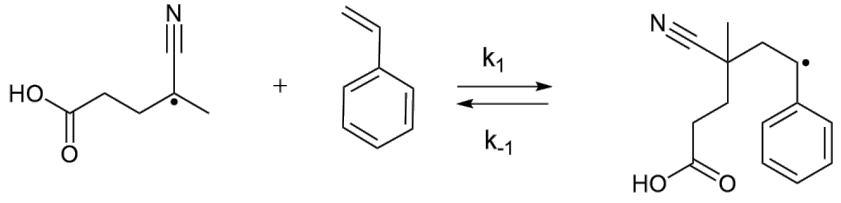

Figure 37: Propagation.

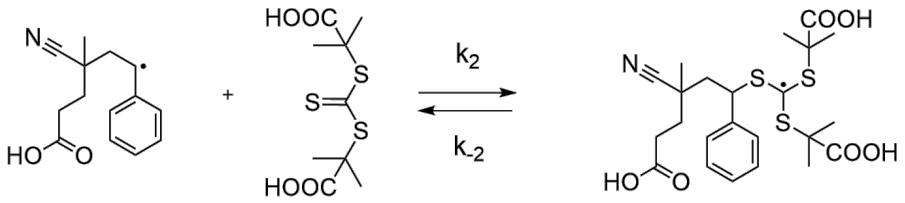

Figure 38: The RAFT pre-equilibrium first step. This step is also in equilibrium with the second step depicted in figure 39

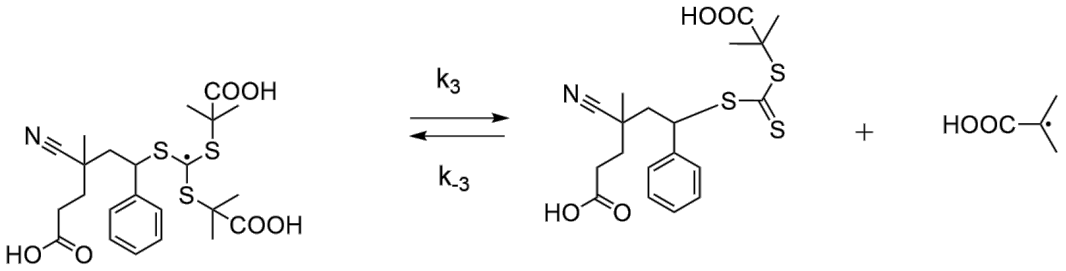

Figure 39: The RAFT pre-equilibrium second step. This step is also in equilibrium with the first step depicted in figure 38

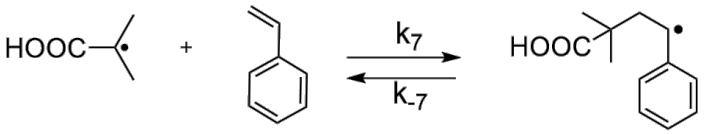

Figure 40: Re-initiation.

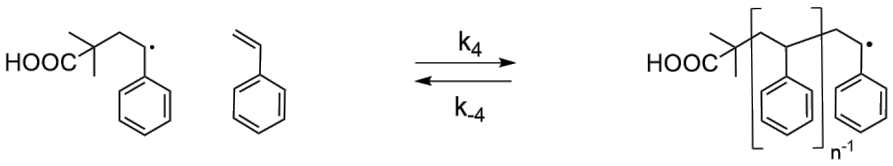

Figure 41: The RAFT propagation with the re-initiated chain growth.

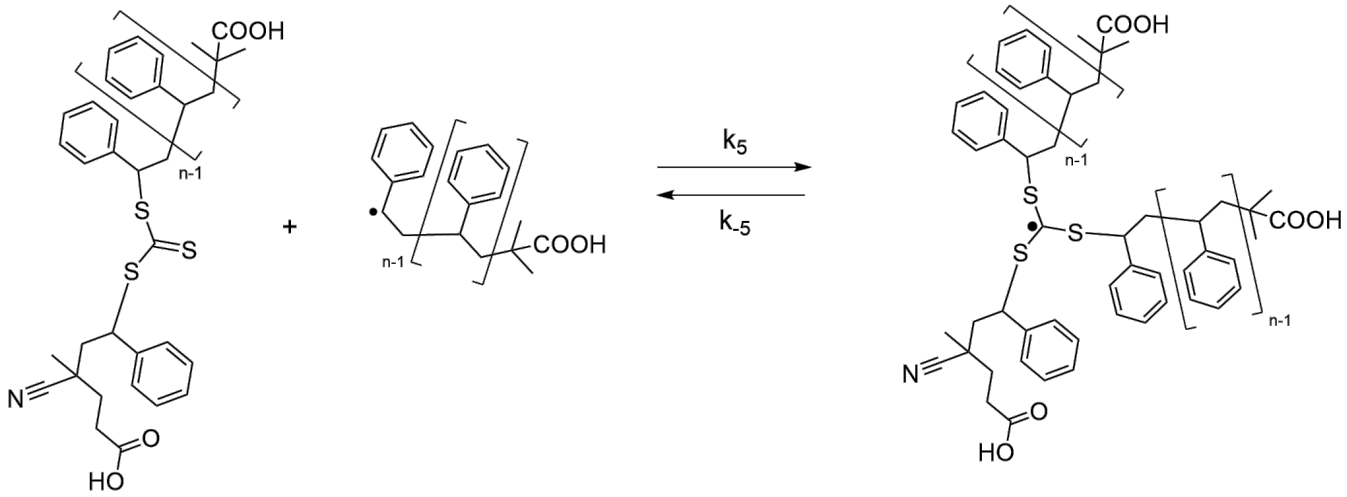

Figure 42: The main RAFT equilibrium step. This equilibrium is also produces radical chains that are capable of growing by radicalizing the present monomers and the reattach again to the RAFT-agent.

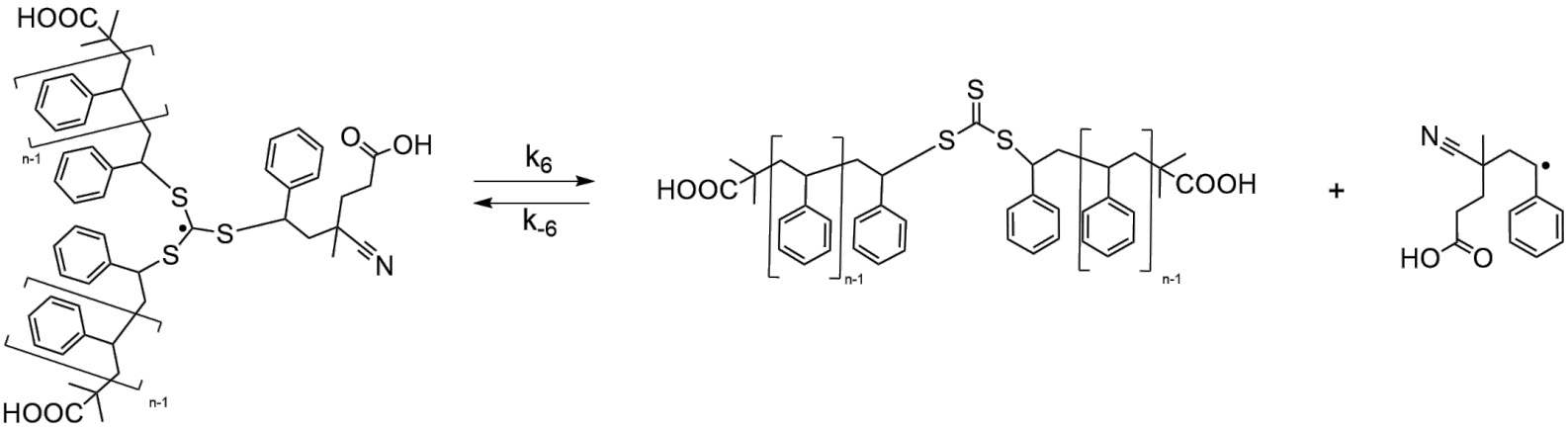

Figure 43: The initiation step where the initiator is split up in radicals.

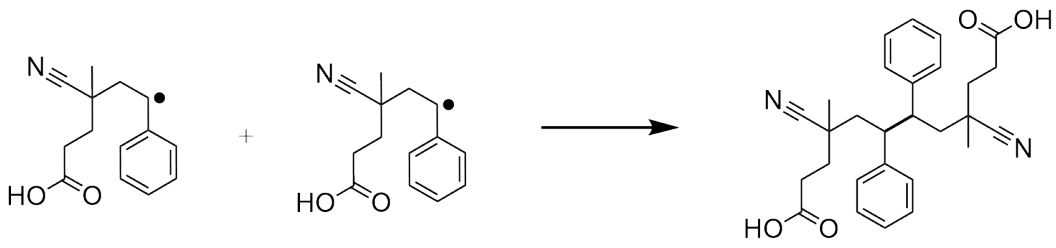

Figure 44: Termination through recombination. This process is in RAFT mechanisms mostly depicted as general radical species recombining. However, due to the nature of this RAFT-agent it is likely that it is the initiator which is recombining in the termination step due to the distribution of molecular weight.

A.7 Quick, quantitative hetero-nuclear correlation (QQ-HSQC) spectroscopy

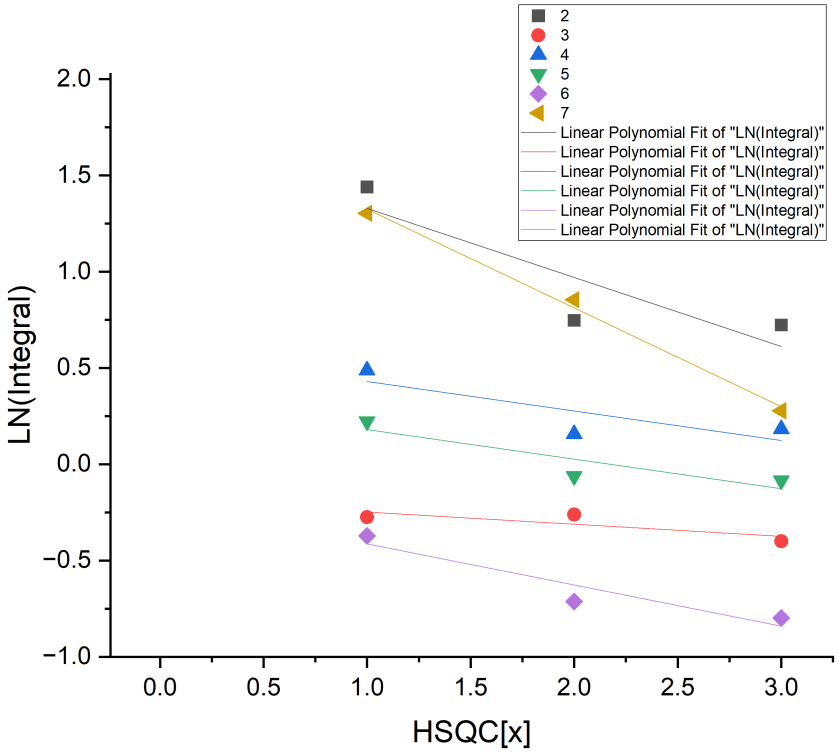

Figure 45: The HSQC data points plotted on the graph were a linear relationship is clearly visible. The coordinates of the datapoints can be found in table 17, the equation for the linear fit to these data points and the extrapolated $HSQC_0$ data points can be found in table 18

Table 17: Peak integrals of the processed QQ-HSQC spectrum.

$HSQC_1$						
	f2 (ppm)	f1 (ppm)	Width f2	Width f1	Normalized	Absolute
1	6.84	45.2	563.86	1542.51	5.00	5731.52
2	4.18	146.15	289.79	870.13	4.22	4837.38
3	1.93	122.73	282.41	400.2	0.76	867.7
4	1.55	108.71	217.91	830.58	1.63	1864.36
5	1.46	126.14	231.38	1397.49	1.25	1430.08
6	1.28	111.99	163.99	711.93	0.69	792.59
7	0.89	99.19	289.79	1806.19	3.68	4219.69
$HSQC_2$						
	f2 (ppm)	f1 (ppm)	Width f2	Width f1	Normalized	Absolute
1	6.84	45.2	563.86	1542.51	5.000	4041.69
2	4.18	146.15	289.8	870.26	2.110	1707.24
3	1.93	122.73	282.41	400.19	0.770	618.64
4	1.55	108.71	217.91	830.57	1.170	942.08
5	1.46	126.14	231.39	1397.51	0.940	760.22
6	1.28	111.99	163.99	711.96	0.490	393.2
7	0.89	99.19	289.8	1806.23	2.350	1898.49
$HSQC_3$						
	f2 (ppm)	f1 (ppm)	Width f2	Width f1	Normalized	Absolute
1	6.84	45.2	563.86	1542.51	5	2650.89
2	4.18	146.15	289.8	870.26	2.06	1094.56
3	1.93	122.73	282.41	400.19	0.67	356.78
4	1.55	108.71	217.91	830.57	1.2	634.39
5	1.46	126.14	231.39	1397.51	0.92	485.91
6	1.28	111.99	163.99	711.96	0.45	236.4
7	0.89	99.19	289.8	1806.23	1.32	697.43

Table 18: The linear fit to the QQ-HSQC-data giving the $HSQC_0$ integral which is the actual integral of the specimen relative to the reference peak of styrene at 6.84 ppm.

	Linear fit of peaks	fA,n	$HSQC_1$	$HSQC_1$ - $f_{A,n}$	EXP($HSQC_1$ - $f_{A,n}$)
2	y = -0.3586x + 1.6869	-0.3586	1.439835128	1.798435128	6.040187944
3	y = -0.063x - 0.1861	-0.063	-0.274436846	-0.211436846	0.809420398
4	y = -0.1531x + 0.5822	-0.1531	0.488580015	0.641680015	1.899669673
5	y = -0.1533x + 0.3325	-0.1533	0.223143551	0.376443551	1.457093286
6	y = -0.2137x - 0.2002	-0.2137	-0.371063681	-0.157363681	0.854393275
7	y = -0.5126x + 1.8369	-0.5126	1.302912752	1.815512752	6.144225835

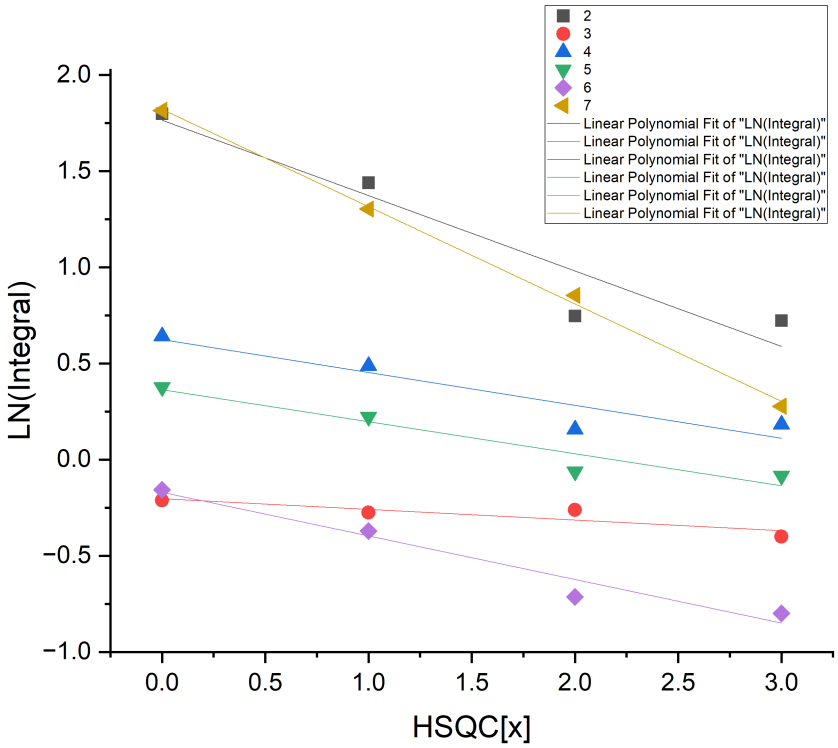

Figure 46

A.8 Diffusion ordered spectroscopy (DOSY)

Figure 47: DOSY resuls for all the polymers.

(a) DOSY of RG17

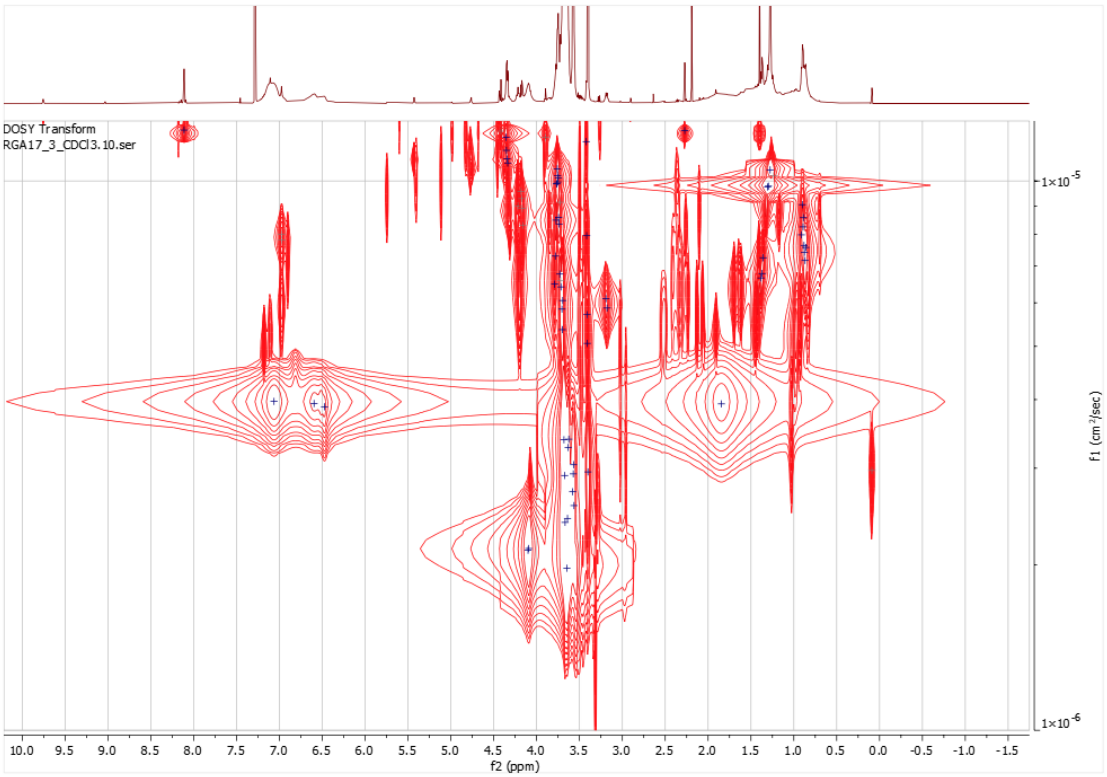

(b) DOSY of RGA

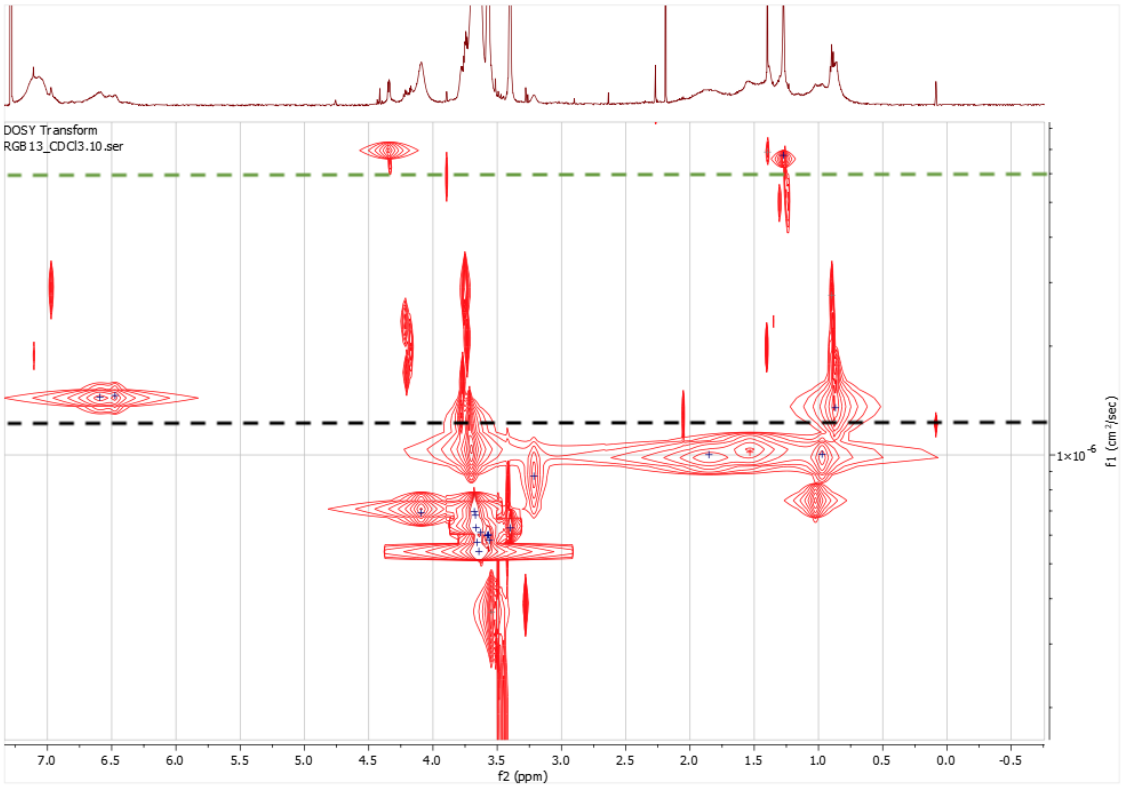

(c) DOSY of RGB

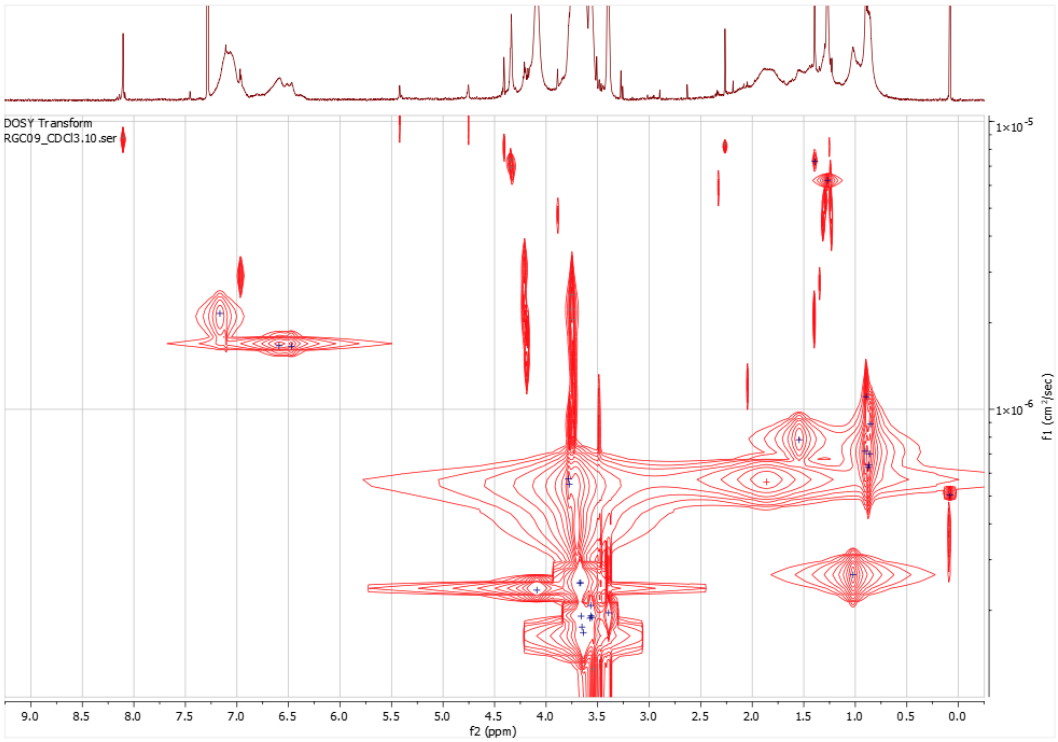

(d) DOSY of RGC

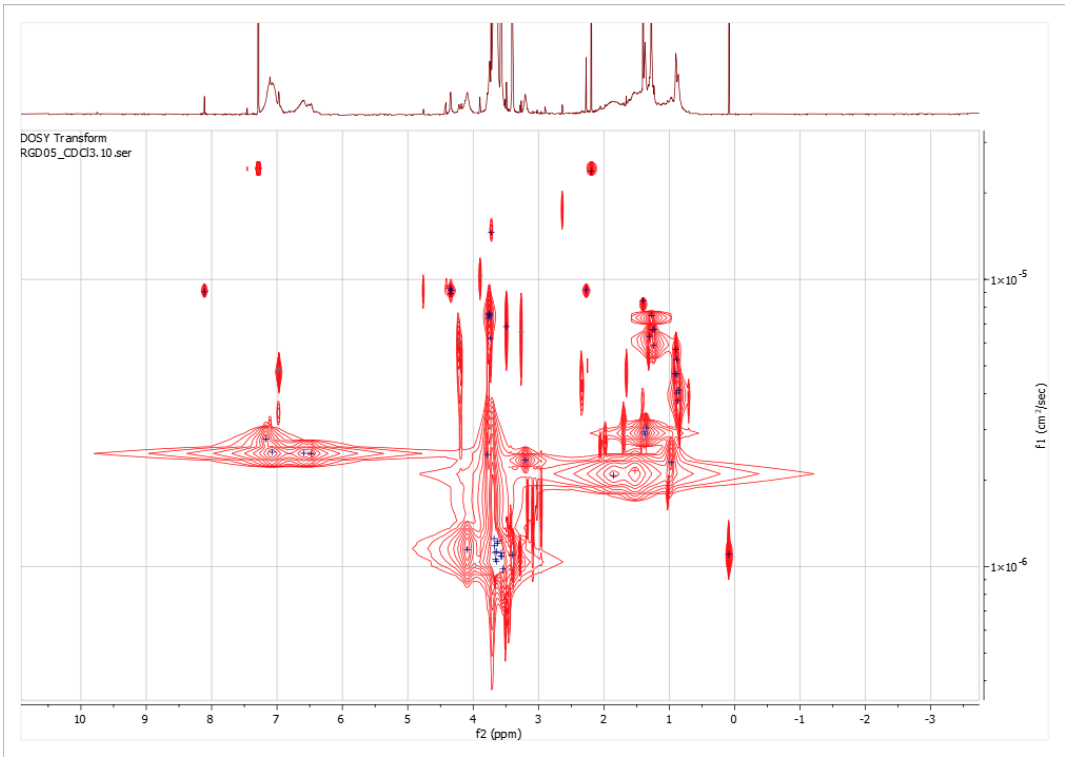

(e) DOSY of RGD

B Appendix II

B.1 TGA-data

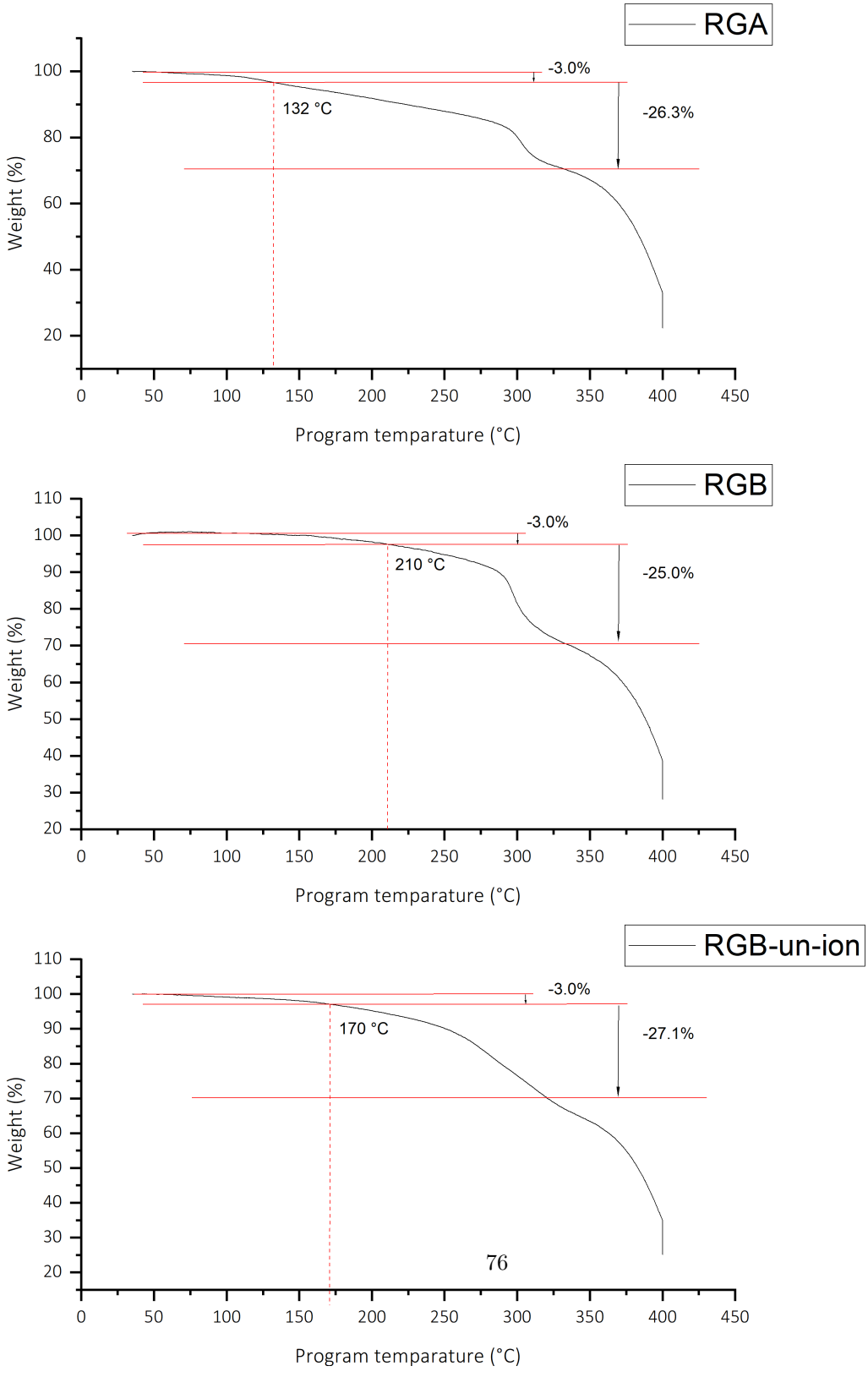

Figure 48: The results of the TGA

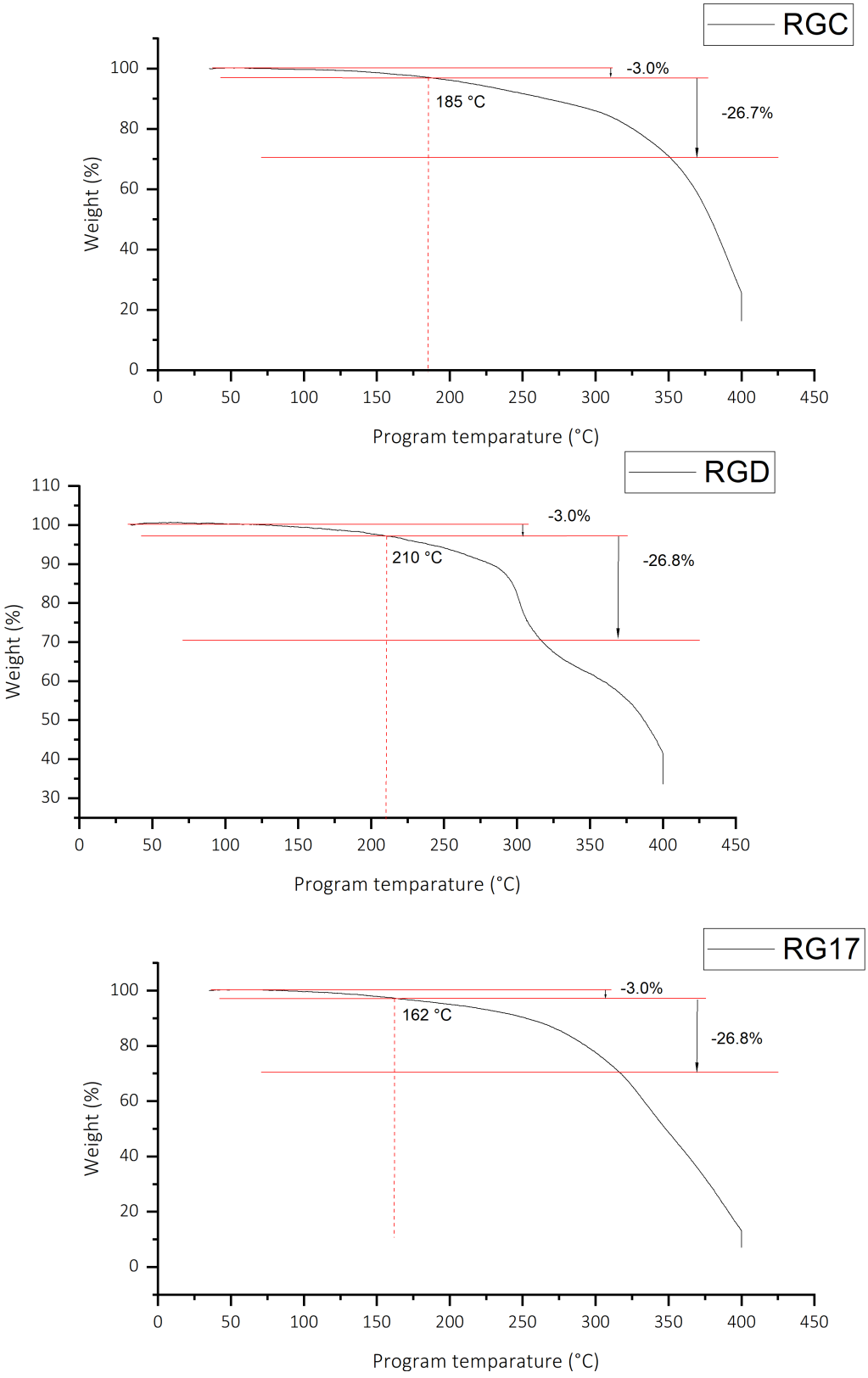

Figure 49: The results of the TGA

B.2 DSC-data

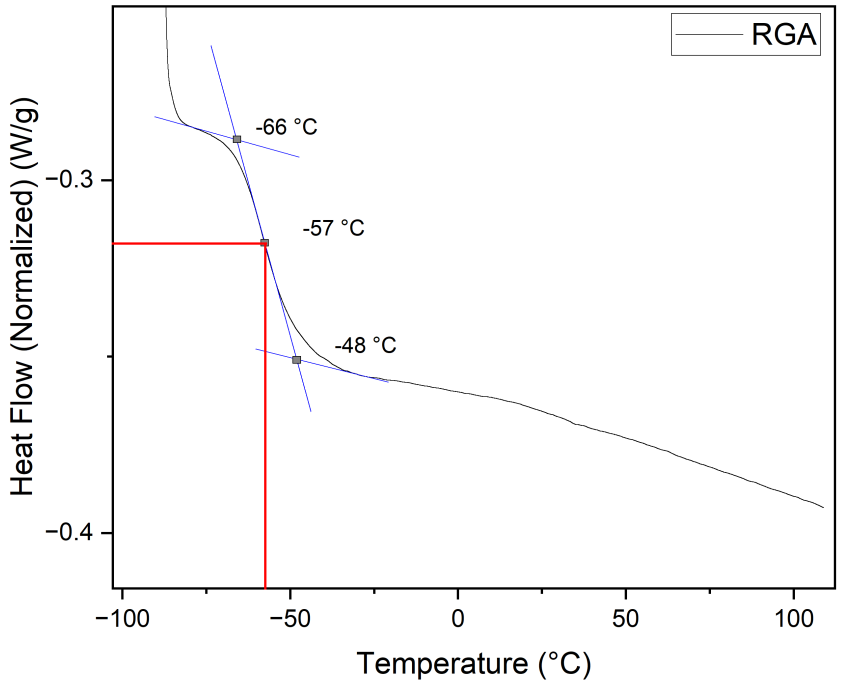

Figure 50: The results DSC for RGA

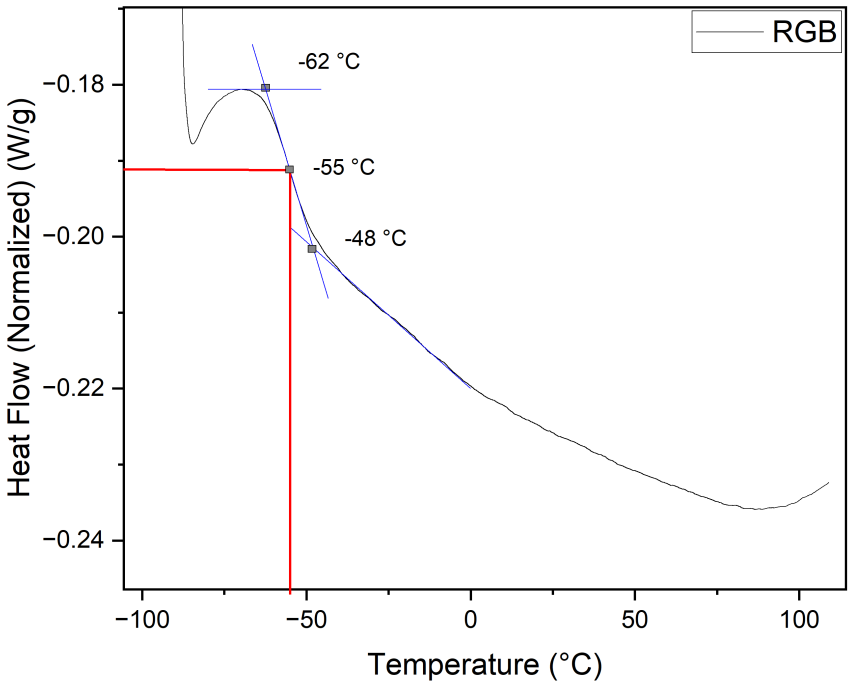

Figure 51: The results DSC for RGB

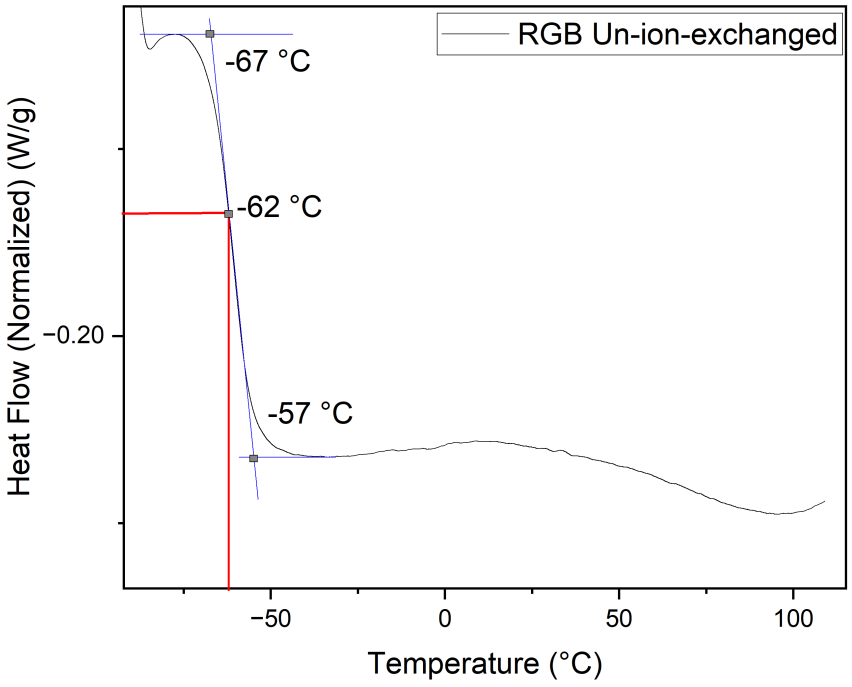

Figure 52: The results DSC for RGB with the Et_3N still present in the polymer

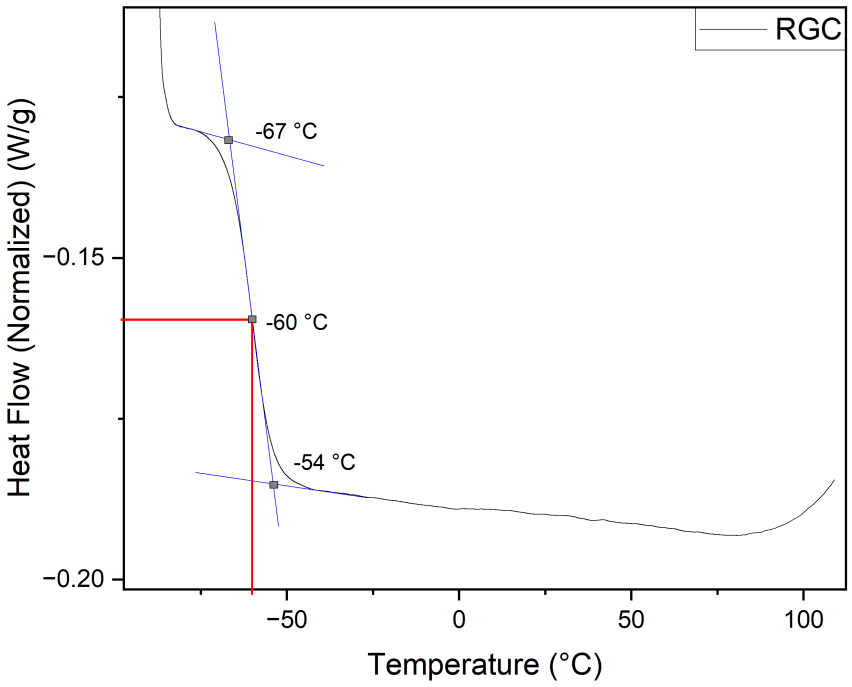

Figure 53: The results DSC for RGC

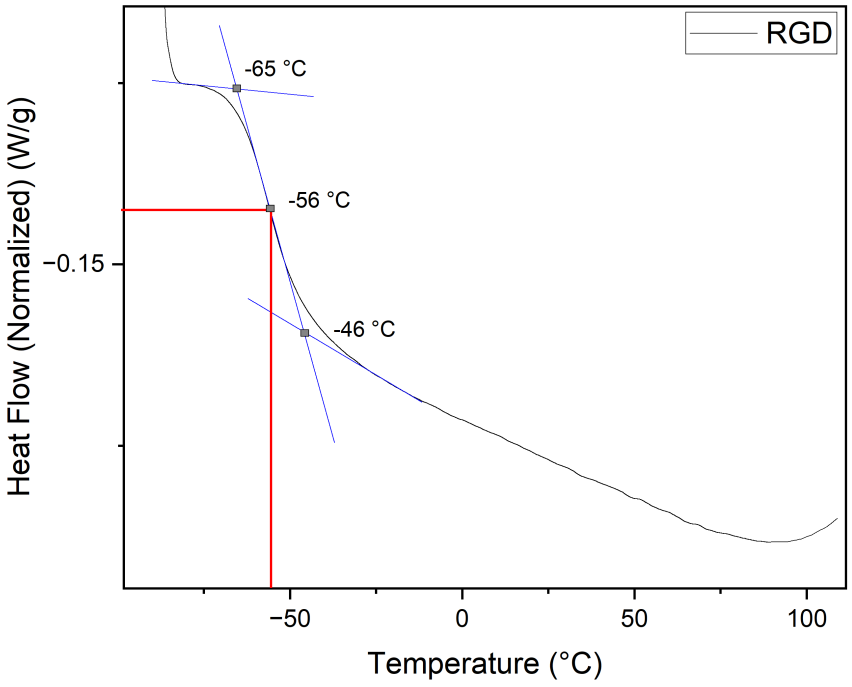

Figure 54: The results DSC for RGD

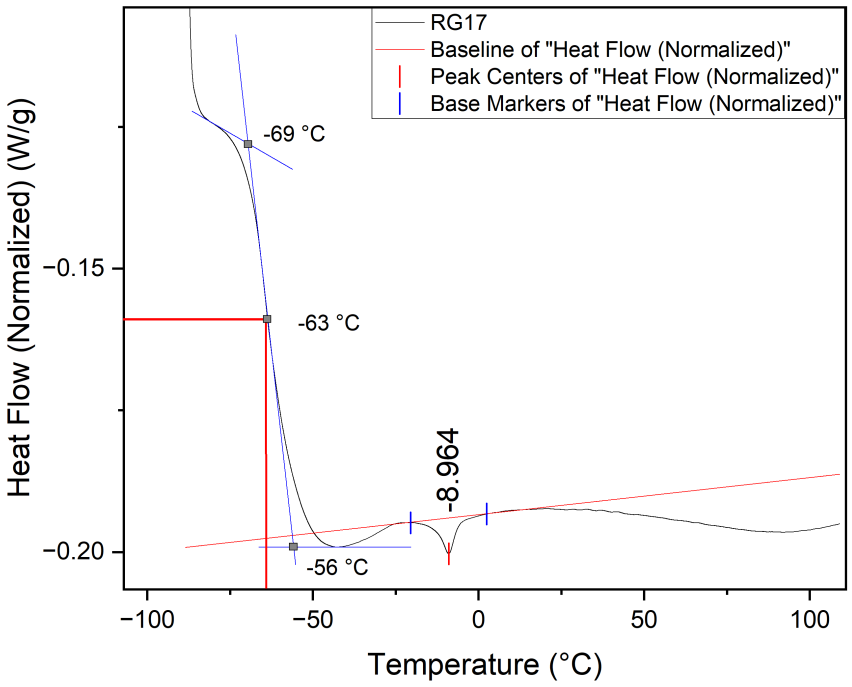

Figure 55: The results DSC for RG17 where the influence of adding AMPS becomes visible since there is molecular relaxation happening at $-8.964\,^{\circ}\mathrm{C}$ which is caused by slow response of the unhindered PEGMA-part

C Electrochemical impedance spectroscopy (EIS) results

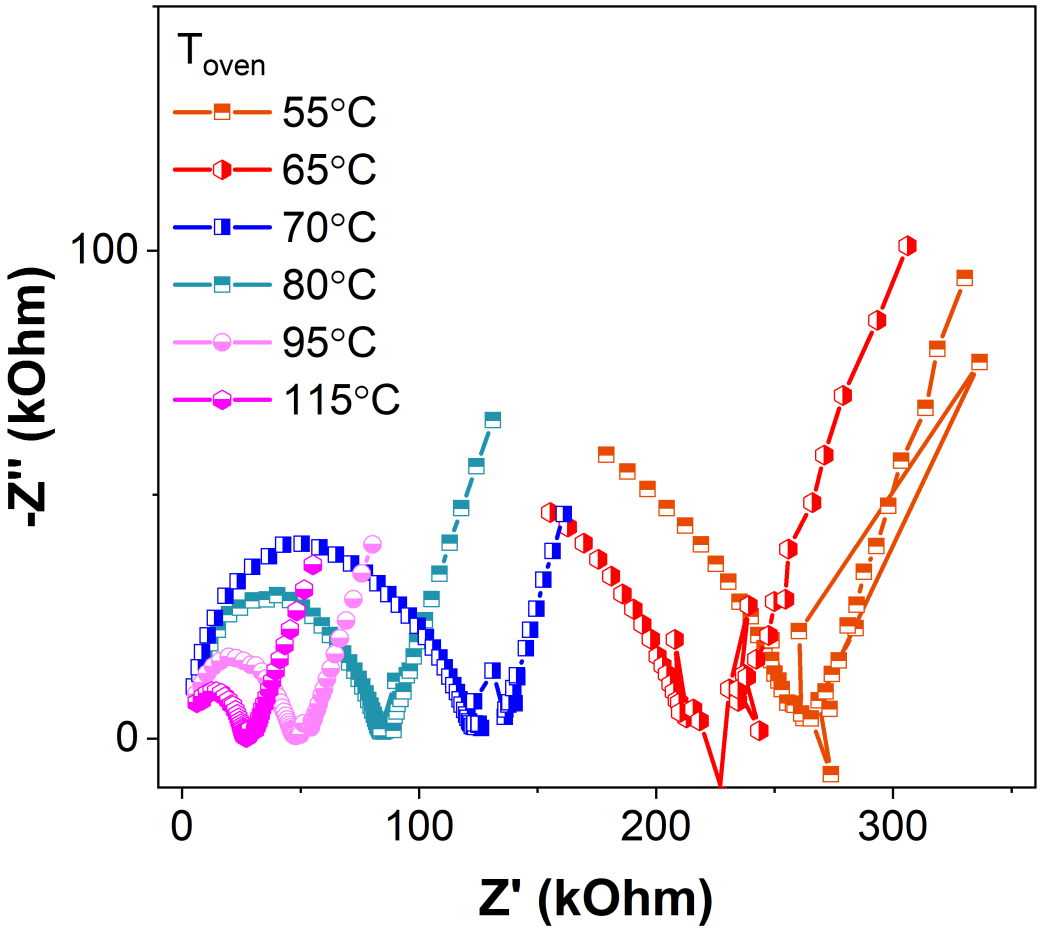

Figure 56: The obtained Electrochemical impedance spectroscopy results of **RGB**. The Swagelok cell was put in the oven for 1 h with a temperature sweep from 55 °C to 115 °C. The temperature of the cell was measured with a heat probe. (**Note:** The temperature of the oven is provided, however, the actual temperature of the cell is 7 °C to 10 °C lower.)
(RGB): Thickness of the membrane as tested is 1.2 mm. The contact area of the membrane is 0.5 cm^2

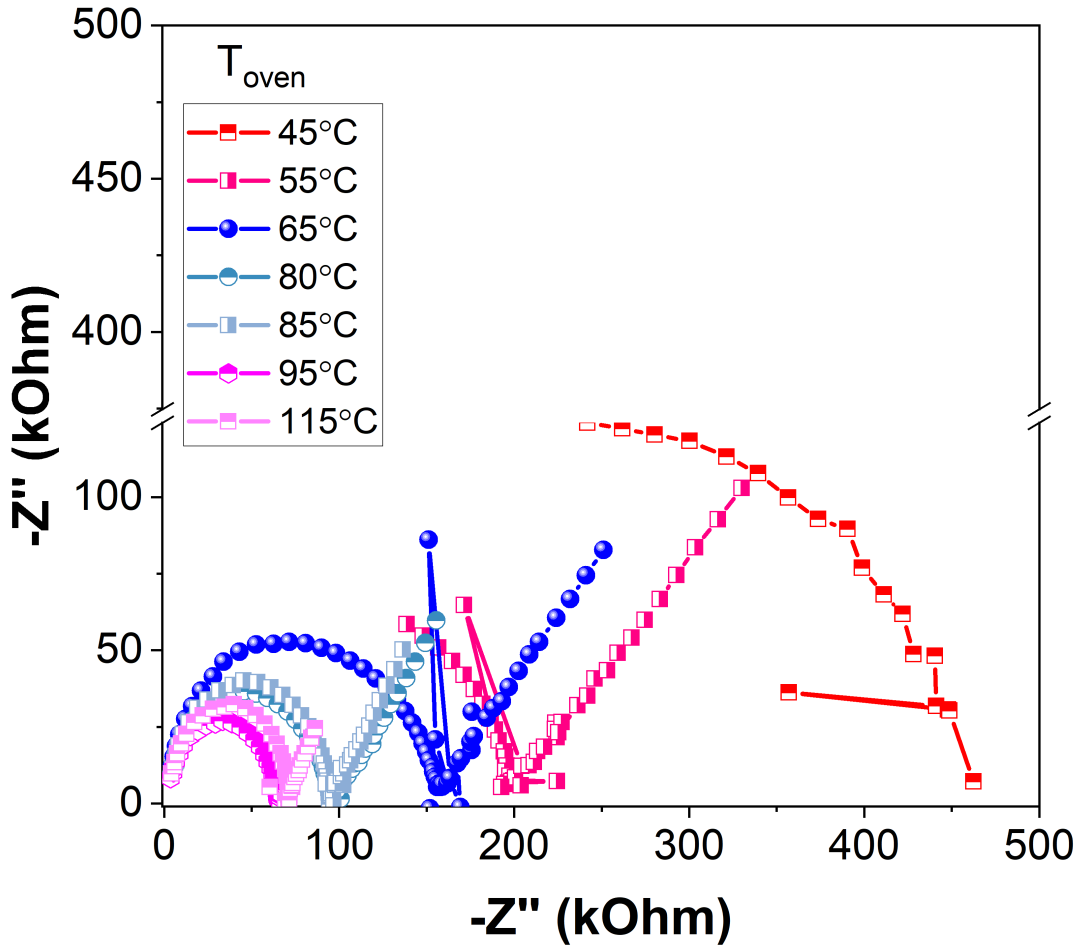

Figure 57: The obtained Electrochemical impedance spectroscopy results of **RGC**. The Swagelok cell was put in the oven for 1 h with a temperature sweep from 55 °C to 115 °C. The temperature of the cell was measured with a heat probe. (**Note:** The temperature of the oven is provided, however, the actual temperature of the cell is 7 °C to 10 °C lower.)
(RGC): Thickness of the membrane as tested is 1.1 to 1.2 mm. The contact area of the membrane is 1.13 cm^2